Materials Science and Engineering B 266 (2021) 115024

Contents lists available at ScienceDirect

Materials Science & Engineering B

journal homepage: www.elsevier.com/locate/mseb

Review

Recent developments in centrifugally spun composite fibers and their performance as anode materials for lithium-ion and sodium-ion batteries

Roberto Orrostieta Chavez [a], Timothy P. Lodge [b], Mataz Alcoutlabi [a,*]

[a] Department of Mechanical Engineering, University of Texas, Rio Grande Valley, Edinburg, TX 78539, USA
[b] Department of Chemical Engineering and Materials Science and Department of Chemistry, University of Minnesota, Minneapolis, MN 55455, USA

ARTICLE INFO

Keywords:
Centrifugal spinning
Lithium ion battery
Anode
Composite nanofibers
Metal oxide
Sodium ion battery

ABSTRACT

Nanofibers (NFs) and composite NFs have been widely used as electrode and separator materials in lithium-ion batteries (LIBs) and sodium-ion batteries (SIBs) due to their high surface-area-to-volume ratio and versatility of their morphologies. The majority of carbon-fibers (CFs) anodes have been prepared by electrospinning and subsequent thermal treatment. Nevertheless, the low fiber yield and safety hazards associated with this method have raised concerns and limited the commercialization of composite CF anodes. Fiber and nanofiber processing methods such as centrifugal spinning can overcome low productivity and eliminate the use of a high voltage to produce fibers. In the present work, centrifugally spun fibers with alloying, transition metal oxides, and transition metal sulfite-based materials are presented and discussed for potential use as anode materials in LIBs and SIBs. Emphasis is given on the centrifugal spinning process and its effects on fiber formation, morphology, and structure of these nanocomposite anodes.

1. Introduction

More than ever, batteries play a crucial role in the performance of electronic devices as society becomes more dependent on portable devices [1]. LIBs have been demonstrated to be the best fit to power portable devices because of their high energy density and long cycle stability [2]. Furthermore, as energy storage technology advances, batteries have been sought by other industries as an alternative to power their devices/machines. One of the best examples is the rise of electric (EV), plug-in hybrid (PHEV), and hybrid vehicles (HEV) as a potential solution to the CO_2 emissions of fuel-powered vehicles. HEVs require a high-power LIB pack, while EVs and PHEVs require a high-energy–density LIB pack to achieve a greater travel range [3]. Power performance and cycle life must also be improved for the future implementation of LIBs in all EVs Moreover, a major deterrent to the application of LIBs in EVs is the flammability (thermal runaway) when they are poorly designed, or when LIBs suffer thermal, electrical, or mechanical abuse [4] Other issues with the commercialization of energy storage technologies include the geographically constrained mineral reserves of lithium combined with the increasing demand for energy storage in large-scale renewable energy technologies (wind, solar, etc.). The relatively low abundance of lithium and its high demand make the depletion of lithium sources a possibility within a foreseeable future [5,6]. Because of this scarcity, potential alternative ions such as sodium are good candidates to replace lithium in larger-scale battery applications. Sodium, in contrast to lithium, is widely recognized as an abundant and low-cost metal [5,7]. Unfortunately, sodium-ion batteries (SIBs) face a distinct challenge due to the large size of the Na-ion (Na^+) [8,6] which prevents intercalation with graphite anodes [5,8,9]. Currently, work is being conducted to achieve the intercalation of Na^+ with graphite. For example, hard carbon (HC) is extensively studied as a potential negative electrode for SIBs [8,6,9] HC is non-graphitizable and has turbostratic domains spaced by curved graphene nanosheets and larger interlayer spacings than the well-defined interlayer spacing in graphite (3.3 Å). Hence, the complex molecular-level structure of HC can reversibly accommodate large size ions such as Na^+ [10]. Moreover, composite materials are being developed to improve the electrochemical performance of SIBs. Among the approaches selected, composite fiber anodes have been explored in some detail.

In this review, metal/carbon (C), metal-oxide/C, and metal-sulfide/C composite-fiber anodes prepared by the centrifugal spinning method and subsequent thermal treatment, and their use in LIBs and SIBs, are discussed. Both binary and ternary composite carbon fibers (CFs) are considered. The use of these ternary composite fibers can alleviate the

* Corresponding author.
E-mail address: mataz.alcoutlabi@utrgv.edu (M. Alcoutlabi).

https://doi.org/10.1016/j.mseb.2020.115024
Received 14 September 2020; Received in revised form 11 November 2020; Accepted 21 December 2020
Available online 18 January 2021

high-volume expansion observed in high capacity metal oxide anodes and alloy-based materials.

1.1. Working principle of batteries

The main active components in a LIB include the cathode, anode, electrolyte, and separator. The schematic in Fig. 1 illustrates the Li^+ transport between the electrodes.

During the charging process, Li-ions move from the cathode through the ionically conductive electrolyte and either intercalate or alloy in the anode. During discharge, the Li-ions move back to the cathode passing once again through the separator, which is permeable to ionic flow but prevents short-circuits in the battery from direct contact of the electrodes [11–13]. The working principle of SIBs is similar, in that Na-ions alloy/dealloy or intercalate/deintercalate with the active material in the anode/cathode [14,9].

Separators based on composite fibers can be fabricated from nonwoven nano/microfibers. Several factors must be considered when designing a separator. Some key requirements include minimal ionic resistance, mechanical and dimensional stability, and electrolyte uptake [12,15]. Currently, polyolefin microporous membranes are the separators used in commercial LIBs because of their electrochemical stability, adequate thickness, and good mechanical strength [16,17]. However, polyolefin separators are known for poor wettability and dimensional instability at elevated temperatures when the battery experiences a high current flow; such dimensional instability could eventually lead to internal short-circuiting and thermal runaway [16,17,11]. Thus, research is also being conducted to overcome these issues by using nonwoven nanofibers as separator materials.

The most used cathode materials in LIBs are $LiCoO_2$ and $LiFePO_4$, which are commercially available in the form of a slurry dispersed on a collector (aluminum foil) [18,19]. Similarly, anode materials such as the commercially available graphite can be prepared in slurry form and coated on a copper current collector (copper foil). Graphite remains the dominant anode material for LIBs, because of its flat potential profile, high coulombic efficiency, and good cycling performance. However, alternative anode materials with theoretical capacities higher than that of graphite (372 mAh g^{-1}) are being studied to satisfy the demand for superior energy storage devices. Slurry-based anodes possess the advantage over binder-free anodes of being loaded with higher percentages of active materials, which determines the energy density of the electrode. Moreover, a conductive agent that improves the transport of electrons (e.g., carbon black), and a polymer binder that maintains the slurry paste adhered to the current collector, can be added to the active material to improve the performance of the electrode [6]. Homogeneous slurries can be prepared with a high loading of active material (>70%) and dispersed on the copper collector. Nonetheless, slurry-based electrodes face challenges of their own. If a binder does not maintain the slurry in contact with the current collector, the active material will gradually lose physical contact with the current collector [20]. Loss of physical contact is usually caused by the volume change during the insertion/disinsertion of Li^+ into the anode. In slurry-based anodes, the nanostructure of the active material can be modified to buffer any volume change of the electrode.

Nanofibers, on the other hand, can endow active materials with enhanced nanostructures and modify the structure of the matrix in which they are dispersed to further improve the volumetric buffering capabilities of the anode. Thus, composite fibers with high active material loading and good dispersion in the carbon-fiber matrix can result in binder-free anodes with improved electrochemical performance compared to slurry-based anodes. Centrifugal spinning (CS) has proven to be capable of producing beneficial structures such as hollow fibers and porous fibers that facilitate Li^+/Na^+ transport since the fibers can shorten electron pathways and increase ion accessibility [21–25].

Moreover, nanostructured materials with high surface area and a thin and stable solid electrolyte interface (SEI) layer can result in electrodes with high charge–discharge rates, thus improved the specific power and energy density of the battery [26–28]. In fact, mitigating the

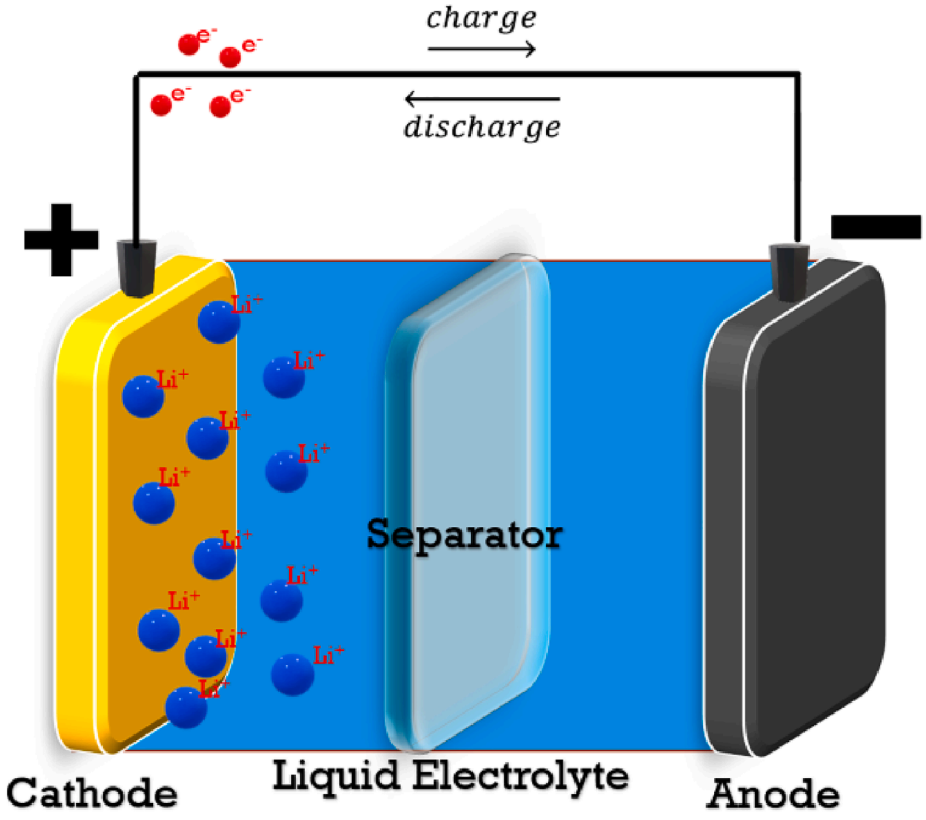

Fig. 1. Schematic with active components of lithium-ion batteries.

effect of SEI layer formation on the irreversible capacity and electrochemical performance of LIBS has been a challenge for the scientific community [29]. During the SEI formation process, not only the constituents of the anode material are consumed, but also Li-ions [29,30]. Another aspect that causes the formation of SEI is the use of anode materials with higher working voltage than that of the electrolyte. The lower and upper working voltages of electrolytes are known as the lowest unoccupied molecular orbital (LUMO) and the highest occupied molecular orbital (HOMO), respectively. For commercial organic electrolytes such as dimethyl carbonate/diethyl carbonate (DMC/DEC), the LUMO and HOMO have values of 1.2 and 4.2 eV, respectively [31]. When the working voltage of an anode is below the LUMO of its electrolyte, such as in the case of graphite (0.2 V vs Li/Li^+), the electrolyte will be reduced to reach the anode's working voltage and form the SEI [2,30].

Currently, most of the work reported on centrifugal spinning focuses on the preparation of new materials and their use in different applications; further investigation is needed to identify the effect of processing parameters on the mechanical properties and performance of the fibers [32]. In the following section, we explore how binder-free composite anodes and nonwoven membranes can effectively perform and overcome some of the issues encountered in conventional electrodes and separators for LIBs.

1.2. Application of nanofibers in lithium-ion batteries

Flexible binder-free anodes can be prepared with active material (e.g., nanoparticles) embedded in a carbon-fiber (CF) matrix to produce composite CFs. The use of CFs can decrease the cost of battery fabrication because CFs can directly be used as binder-free anodes without the need for conductive fillers or a current collector (copper foil) [33,34]. The elimination of copper foil is especially beneficial since current collectors are major contributors to the environmental burden caused by the production of batteries [35]. Moreover, composite CFs have attracted attention due to their high surface-area-to-volume ratio and high-rate of Li^+ insertion when structural or surface defects are present [36,34]. The specific surface area of the CFs can be enhanced by different preparation methods. For example, the fiber morphology has been improved by the generation of pores, which can increase the clearance space for volume change and Li^+ diffusion on the electrode surface [37]. Additionally, non-calcinated non-woven fibrous mats can also be used as battery separators To improve efficiency, the separator must feature small volume and high porosity [38,39]. Non-woven fibrous mats usually have a thickness between 100 and 200μ m and base density between 9 and 30 g cm^{-2} [40]. Fiber-based battery separators must have a fiber diameter smaller than 5μ m [40]. Fibers with a larger diameter can cause the presence of locally open spaces that could not properly prevent short circuits between the electrodes [40]. For this reason, non-woven membranes are mainly used as a support layer for separators impregnated with gel polymer electrolytes [41]. Nonetheless, fibers with smaller diameters can be prepared with current manufacturing technologies such as electrospinning and centrifugal spinning. PVDF is the most commonly used polymer in the preparation of separators, but polymers such as PAN and PMMA are also implemented to improve the thermal stability and mechanical strength of non-woven membrane separators [42,43]. Moreover, composite fibers can also be prepared to improve the performance of fiber-based separator membranes. Some commonly added fillers to the polymer fiber matrix include Al_2O_3, SiO_2, and TiO_2. Such particles can increase mechanical strength, thermal stability, and ionic conductivity [17,43]. Thus, the ability to manipulate the structure of fibers not only benefits the performance of electrodes but also the separator.

1.3. Anode materials for Li-ion batteries

Graphite is the primary commercial anode material for LIBs owing to its flat potential profile, stable capacity during prolonged charge/discharge cycles, and high coulombic efficiency. However, the graphite anode exhibits relatively low theoretical capacity (372 mAh g^{-1}) and low specific power caused by the low Li^+ diffusivity (10^{-8} cm^2 s^{-1}) in the carbon structure [44]. Extensive research efforts have been made to overcome the deficiencies of graphite anodes. Metals, semimetals, metal oxides, and metal sulfides have been proposed as alternative anode materials to address the challenges facing the commercial graphite anode. These materials are based on lithiation-delithiation mechanisms such as intercalation-deintercalation, alloying-dealloying, and conversion reactions [26,28]. The intercalation, alloying, and conversion reaction mechanisms, which determine the behavior of active materials during the charge/discharge cycles, will be discussed in the following section. Then, a brief overview of other methods to produce separator membranes and CFs will be provided.

1.3.1. Li^+ intercalation – Deintercalation reaction

Transition metal oxide and metal sulfide anodes exhibit improved electrochemical performance compared to graphite anodes due to their redox catalytic properties [45]. Anodes based on the Li^+ intercalation-deintercalation reaction (e.g., graphite, layered structures of TiO_2, MoO_2, and metal sulfides such as MoS_2, WS, TiS_2, etc.) undergo a process in which the ions are incorporated as a guest within the host crystal lattice without destroying its structure Even though the limited intercalation sites lead to relatively low capacities, the intercalation mechanism is capable of retaining capacity over many cycles because it does not modify the structure of the host material [18]. Nonetheless, the insertion of ions into these metal oxides results in a high volume expansion, which ultimately leads to loss of contact between the active material and current collector of the electrode [22]. In this regard, composite CFs possess an advantage since their conductive structure functions as a current collector as well.

1.3.2. Alloying-Dealloying reaction mechanism

Anode materials based on the alloying mechanism are not limited by their atomic framework; this allows these types of materials to host a larger number of Li-ions [18]. Thus, since the ions break the bonds of the hosting material, higher specific capacities are achieved. Silicon, for example, is capable of forming metallic alloy phases such as $Li_{13}Si_7$, $Li_{13}Si_4$, $Li_{10}Si_3$, and $Li_{22}Si_5$, among others [46], with $Li_{22}Si_5$ (or $Li_{4.4}Si$) having a theoretical capacity of 4200 mAh g^{-1} [46].Nonetheless, the addition of 4.4Li atoms per Si atom leads to an increase in volume to >400% of the Si-anode alone. Hence, even though alloying reaction materials are in principle capable of offering higher specific capacities, their commercialization has been deterred due to their large volume changes occurring after repeated charge/discharge cycles.

Metal oxides can react with Li^+ via alloying, insertion, or conversion mechanisms. In alloying-based metal oxides, lithium oxide and metal are formed in the initial lithiation cycle. In subsequent cycles, the newly available metal alloys with lithium. For example, chemical reactions (1) and (2) show the alloying reaction of SnO_2.

$$SnO_2 + 4Li^+ + 4e^- \rightarrow Sn + 2Li_2O \quad (1)$$

$$Sn + 2Li_2O + 4.4Li^+ + 4.4e^- \leftrightarrow Li_{4.4}Sn + 2Li_2O \quad (2)$$

In this reaction, a steady reversible capacity is achieved once the formation of lithium oxide has been completed (reaction (1)) by exhausting the oxygen in tin oxide [47] In the subsequent lithiation cycles, the newly formed inactive lithium oxide no longer reacts with the Li^+. However, Sn is now capable of alloying with the remaining available Li^+ supply (reaction (2)).

Despite their large volume expansion, materials based on the alloying mechanism are extensively sought after because of their greater specific capacities. Multiple approaches have been explored to alleviate the strains caused by the volume expansion of the electrode. It has been shown that the large volume change is an intrinsic characteristic of

materials that react based on alloying, and attempts to repress this volume change will come at the price of a lower capacity and lower reversibility [48]. For composite CFs, one of the approaches used to allow volume expansion of the silicon or other metalloids without highly increasing the overall anode volume is the production of porous or hollow structured fibers. For example, porous Sn/SnO_x nanoparticles were successfully inserted in the pores within CFs [49]. This allows free space within the pore to be filled by the active material when it expands. In another example, Si nanoparticles were encapsulated in folded graphene cylinder-like structures [49]. The folded graphene network not only increased the overall conductivity of the CFs but also buffered the volumetric expansion of silicon that provoked mechanical stresses that in turn lead to the pulverization of fibers. Fibers with porous structures have been extensively used to buffer the volume change of high capacity anodes. In this review, porous fibers fabricated by centrifugal spinning will be discussed.

1.3.3. Conversion reaction mechanism

Transition metal oxides based on a conversion mechanism (redox reaction) are of great interest for anode materials. During the conversion reaction, the formation of decomposed lithium oxide (Li_2O) is accompanied by the formation of metal nanoparticles via oxidation–reduction reactions [26]. This mechanism can be illustrated as follows [50]:

$$M_xO_y + 2yLi^+ + 2ye^- \leftrightarrow yLi_2O + xM \quad (3)$$

During a conversion reaction, the ability to partially reversibly decompose Li_2O back into a metal oxide leads to high reversible capacities and high energy densities [26]. Unfortunately, metal oxide anodes based on a conversion reaction mechanism suffer from low coulombic efficiency during the first cycle, unstable SEI layer formation, large potential hysteresis, and capacity fading during cycling [51]. Several methods have been used to improve the electrochemical performance of metal oxide and metal sulfide-based anodes, such as the use of nanostructured metal oxide/metal sulfide anode materials and metal oxide/carbon nanocomposites.

1.4. Preparation methods of fibers

In this section, we discuss some of the top-down processing methods capable of producing fibrous structures for battery applications with emphasis on the centrifugal spinning method. These methods include melt blowing, bicomponent fiber spinning, phase invention, electrospinning, and centrifugal spinning. Short introductions to their production procedures and working mechanisms will be presented with emphasis on the use of fibers in battery applications.

1.4.1. Melt blowing

Melt blowing is a process in which a molten polymer is extruded through a small die and stretched by high-pressurized hot air to form microfibers (Fig. 2) [52]. The technology was first developed by the American Naval Research Laboratory and further designs such as Exxon's commercial-scale melt blowing mechanism emerged thereafter [53]. In this method, a typical fiber diameter range between 0.5 and 2μ m can be produced [53,52,54].

One of the main advantages of melt blowing is that there is no need to use a solvent to liquefy the polymer. Thus, the production cost and environmental impact are reduced [52]. For this reason, melt blowing represents a relatively low-cost manufacturing process to produce separators. The implementation of melt blowing has been proposed to fabricate thin, but strong, separators with materials such as polyesters, polyamides, and polymethyl pentene [55]. Of these polymers, polymethylpentene showed tolerance to high temperatures while polyester and polyamide exhibited excellent dimensional stability at high temperatures [55]. Finally, novel technologies are emerging to enable the production of fibers and nanofibers by blow spinning. This hybrid

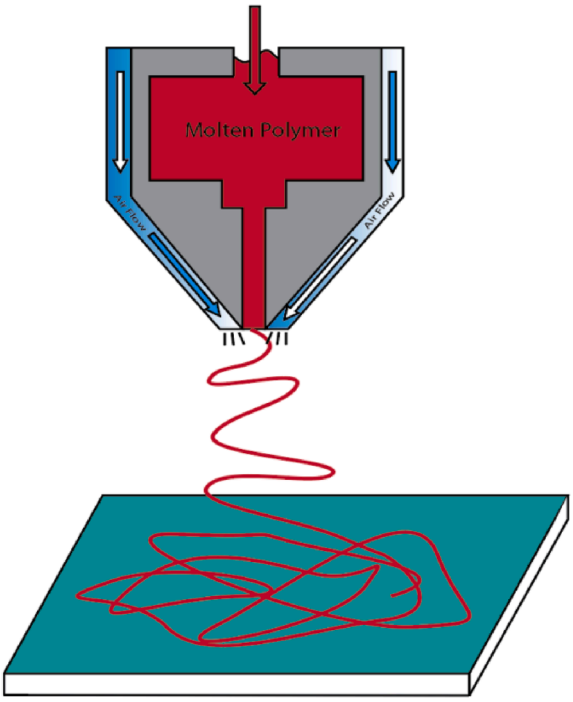

Fig. 2. Single-orifice melt-blowing process.

approach combines electrospinning with melt-blown spinning. In this process, polymer solutions, with or without active materials, are prepared using volatile solvents. A high-speed airflow is then applied alongside a needle where the solution is being injected. The airflow forms the solution jet that ultimately forms into fibers [56,57]. Although this method brings solvents back into the process, blow spinning can produce fibers with a smaller average diameter than melt blowing, ranging from 100 to 1000 nm, thus making them appealing for battery applications [56,57].

1.4.2. Bicomponent fiber spinning

In the biocomponent fiber spinning process, two melted polymers are co-extruded through a coaxial spinning head, or nozzle, to form filaments with designed cross-sectional profiles [58]. Fig. 3 shows a schematic of the fiber melt spinning line.

Among the available cross-sectional profiles, side-by-side, core/sheath, and islands-in-the-sea are the most common (Fig. 3) [59]. These profiles can be obtained by simply changing the spinning head die. This versatility in cross-sectional profiles can potentially enable optimization of fiber parameters such as mechanical strength, surface area, and thermal stability. For example, unidirectional carbon fibers were produced by the bicomponent fiber spinning process and subsequent thermo-chemical stabilization and carbonization of the polymer fiber precursor (Fig. 4).

In battery applications, hollow and finned fibers are remarkably attractive since they increase surface area. Thus, this processing method could also be explored to produce nonwoven fiber membranes for use as battery separators. However, some challenges must be overcome before achieving the manufacturing capability to produce these complex CFs profiles. To begin with, fibers with these cross-sectional profiles have a diameter ranging between 0.5 and 20μ m [60] and, as mentioned above, fibers used as separators must have an average diameter of$<5\mu$ m. These novel structures indeed increase the surface area of the fibers, but they remain too large for battery applications. However, the reduction of their dimensions for the benefit of battery applications is a goal worth exploring.

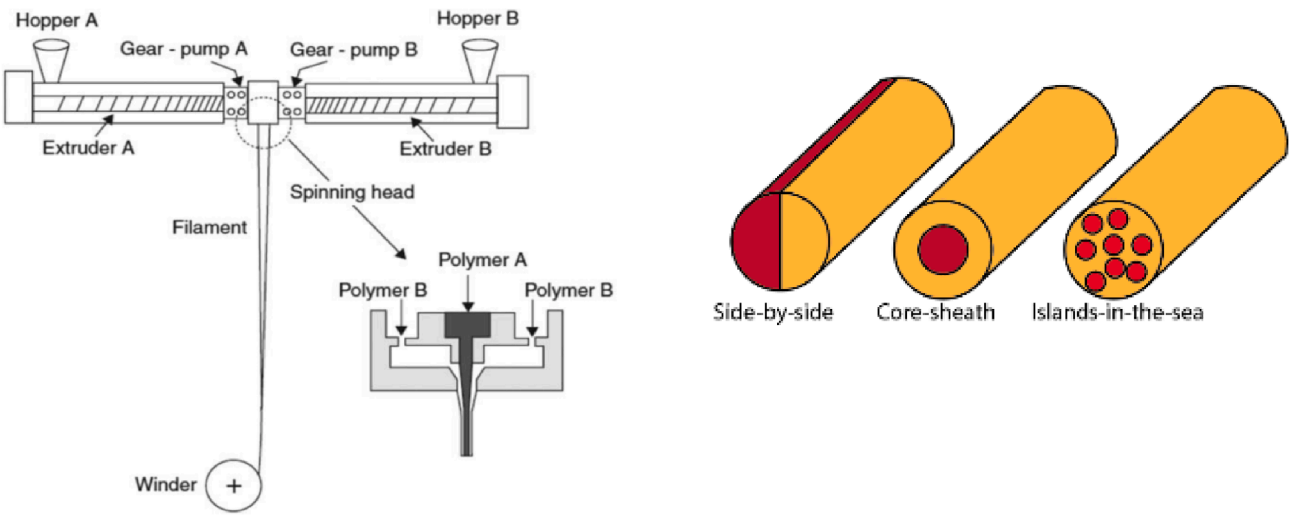

Fig. 3. Schematic of a bicomponent fiber melt spinning line. After Naeimirad et al. [59] with permission.

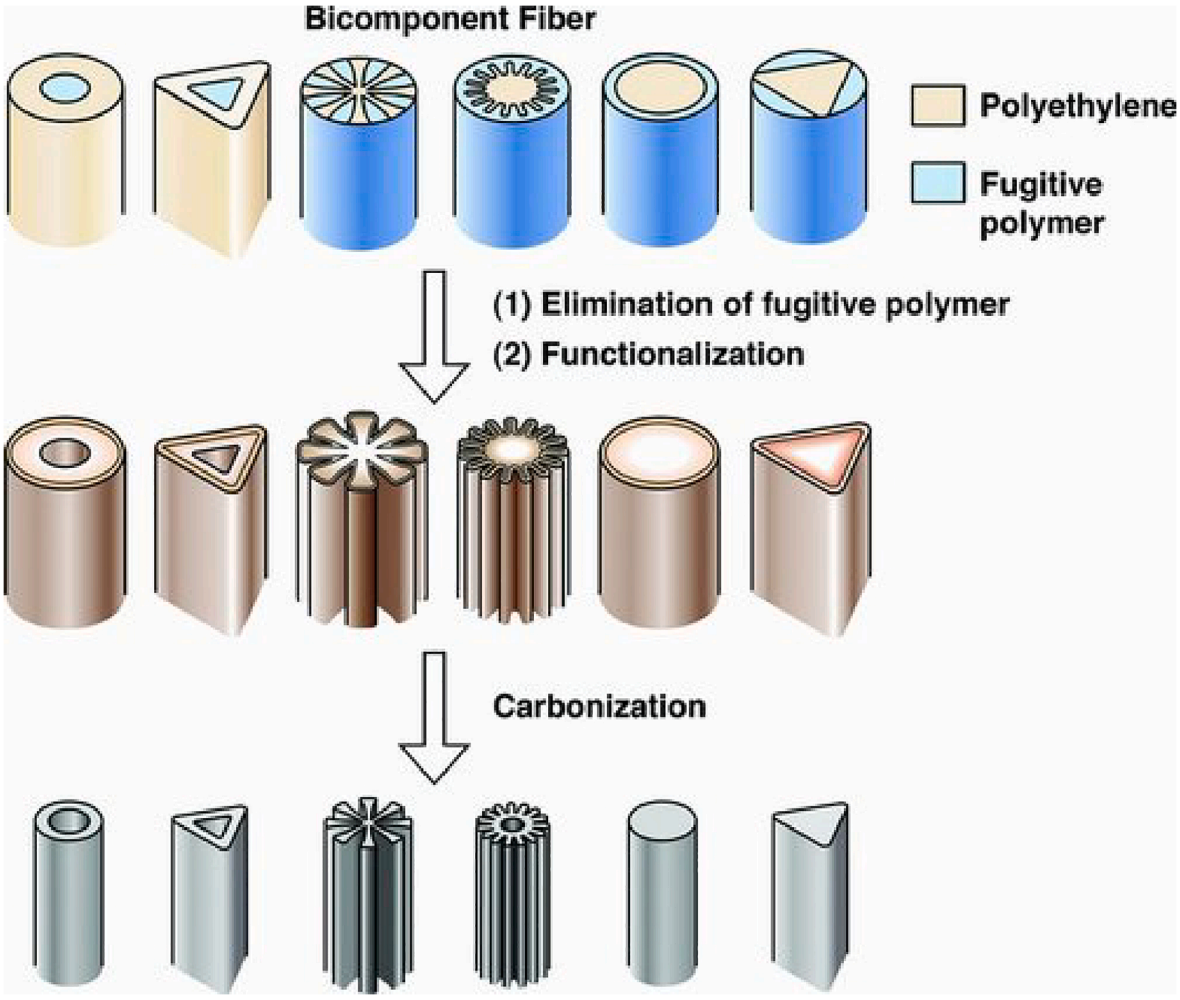

Fig. 4. Schematic describing the method for creating novel CF structures. After Hunt et al. [60] with permission.

1.4.3. Phase inversion: NIPS & TIPS

Phase inversion is a mainstream method to prepare membranes because it can conveniently be adapted for large scale production [61]. However, it involves the implementation of large amounts of organic solvents which are a safety hazard due to their toxic and/or flammable nature [61]. The two main types of phase inversion are thermally induced phase separation (TIPS) and non-solvent induced phase inversion (NIPS). During the TIPS process, a thermodynamically unstable polymer solution forms two phases, one being polymer-rich and the second being polymer-lean [62]. The phase separation process is

induced by either cooling below the binodal solubility curve or by adding an immiscible solvent to the solution [63]. After removing the solvent and drying the polymer-rich and polymer-lean phases, a porous structure is formed due to the difference in density between the two phases [62]. Similarly, during NIPS, a homogeneous dope solution is exposed to a coagulation bath where the solution becomes thermodynamically unstable. The unstable solution then traverses a binodal curve which leads to a polymer-rich and polymer-lean phases that become the membrane structure and pores [64]. Membranes manufactured via phase inversion are used in applications such as food industries, wastewater treatment, and energy storage. Recently, polymer fiber membranes have been developed by the TIPS method for use as separators in LIBs. For example, PVDF/PAN fibrous membranes have been produced via TIPS with controllable morphology (pore size), tensile strength, thermal stability, electrolyte uptake, and ionic conductivity via composition of PAN:PVDF ratios [65]. In that work, the results showed that PAN:PVDF separators enhanced the resistance to shrinkage due to high temperatures (160 °C) although the ionic conductivity decreased from ~3.5 mS/cm in the 100% PVDF separator to ~2.0 mS/cm in the PVDF70/PAN30 blend. Moreover, the phase inversion process also enables the production of composite membranes such as Al_2O_3/PVDF-HFP, and PVDF/PAN/SiO_2 for battery separator applications [66,67]. For these composite membranes, a PVDF70/PAN30 with 1 wt% SiO_2 separator exhibited an improved ionic conductivity compared to the PVDF separator [67].

1.4.4. Electrospinning

The electrospinning process has been known since 1900 when it was first introduced by Cooley [68]. Electrospinning is capable of producing fibers with dimensions down to the nanoscale, but it was not until the 1990s that the nanotechnology field realized the potential of using fibers [69]. Today, the fabrication of nanofibers and microfibers via electrospinning is broadly employed at the laboratory scale because of its simplicity, cost-effectiveness, and versatility [70]. Moreover, electrospinning possesses unique advantages such as improved dispersion and tangential alignment of nanowires and single-walled carbon nanotubes (SWCNTs) within the nanofibers compared to other fiber spinning methods [71]. During electrospinning, a high voltage is applied to a needle from which the polymer solution (or melt) is drawn. The charge difference between the solution and collector induces tension forces that eject a thin solution thread and aligns nanofibers with 1D nanostructure. Soon after the solution is ejected, the solvent evaporates and forms micro/nano fibers in the form of a Taylor cone [13,68]. A schematic of this spinning mechanism is shown in Fig. 5. Electrospinning has been widely used to prepare composite membranes and CFs for applications in LIBs and SIBs. [13,72]. In the following section, centrifugal spinning will be discussed and compared to the electrospinning method.

2. Centrifugal spinning

Centrifugal spinning (CS) is a low-cost and operationally safe manufacturing alternative that is gaining momentum in the production of fibers for multiple applications, mainly due to its much higher fiber yield of 50 g/hr compared to electrospinning (0.1–1 g/hr) [32,73]. Moreover, CS overcomes some disadvantages that electrospinning faces such as the use of a high voltage (>10 kV) to stretch the fibers during processing, and solvent limitations due to insufficient dielectric constant [74,75,23]. In CS, centrifugal forces are applied to a polymer solution or melt, to overcome its surface tension and stretch the polymer droplet (jet) to form fibers [23]. The process begins when a fluid is loaded into a spinneret. Then, centrifugal forces are applied to the solution/melt at high rotational speeds resulting in a polymer jet ejected from the needles attached to the arms of a spinneret. This curved jet is subsequently stretched by extensional forces to form thin fibers deposited on the collectors [32,76,23]. Finally, nonwoven fibers are collected in discrete steps to form a multilayered membrane. Fig. 6 shows the CS setup with the spinneret at the center and 8 collectors equally spaced around the spinneret.

While parameters such as viscosity (concentration) and evaporation rate (for solutions) play important roles in the production of both electrospun and centrifugally spun fibers [36,76] temperature (for melts), collector-to-spinneret distance, and rotational speed are parameters that only apply for centrifugal spinning. These CS exclusive parameters enable researchers to have greater control over the centrifugally spun fiber structure. In general, and as expected, it has been observed that lower solution concentrations at higher rotational speeds produce thinner fibers [77]. A further crucial difference between centrifugal spinning and electrospinning is that the drawing forces applied to the solution during centrifugal spinning are not affected by the collection distance as in the electrospinning method due to the distance-dependent voltage [76]. Thus, choosing the optimum collection distance for centrifugal spinning depends only on the solvent evaporation rate. If the

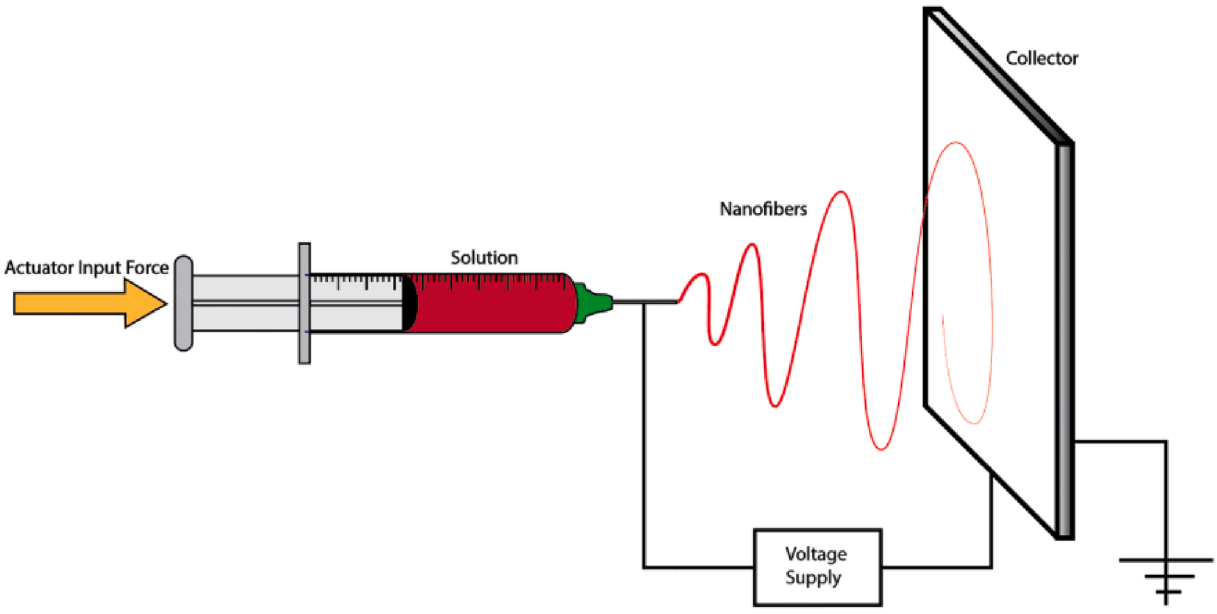

Fig. 5. Electrospinning set up.

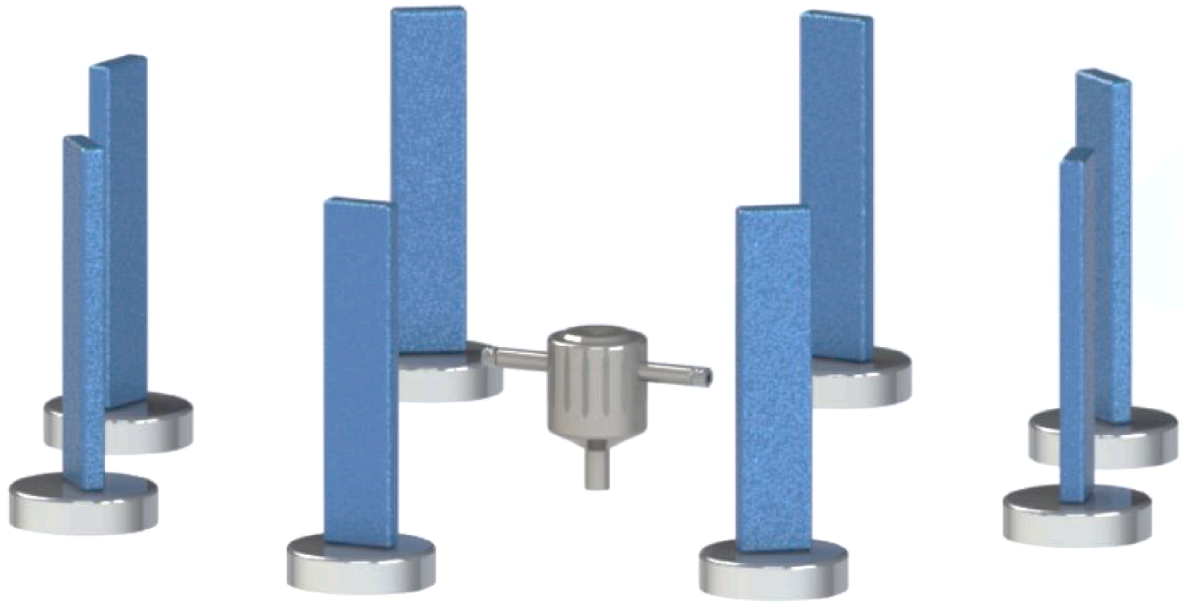

Fig. 6. Centrifugal spinning spinneret and collector schematic.

fiber collection distance is small, the diameter of the fiber will be larger but once the critical distance for solvent evaporation is reached, the collection distance becomes less relevant [76]. In CS, there is a critical rotational speed that must be reached to eject the solution from the spinneret. Furthermore, a second critical angular velocity exists after the solution jet has been initiated. This velocity is reached once the extensional forces on the solution jet have achieved steady-state forces due to the spinneret rotation. As a consequence of this constant pull, the solution exits the spinneret at a higher rate and the jet diameter is reduced well below that of the outlet nozzle [76].

The combination of centrifugal forces with multiple configurations of easily interchangeable spinnerets makes the CF a versatile method with increased material choice, improved production rate, and lower fiber costs through environmentally friendly processes. Centrifugal spinning significantly increases the selection of materials by allowing both non-conductive and conductive solutions to be spun into fibers. Both, polymer melts and solutions are suitable for centrifugal spinning [78,79,36,80]. Solutions with conductive fillers are also suitable for centrifugal spinning because, unlike electrospinning, there is no electric field being applied to the solution/melt during centrifugal spinning [81]. This is one of the advantages of the centrifugal spinning process. Polymer melts such as ultra-high molecular weight polyethylene and polypropylene (PP) have been successfully into centrifugally spun fibers without the need of solvents [36,79]. Keep in mind that the electrospinning of a polymer melt requires a high current to be applied to the melt to overcome the surface tension of the melt and this might result in safety-related issues, especially during the large-scale production of fibers. Conductive solutions are also suitable for the centrifugal spinning polymer solutions with added nonconductive/conductive nanoparticles are also suitable [82]. However, a good nanoparticle dispersion must be achieved prior to centrifugal spinning, otherwise suspended particles in the solution could lead to large nanoparticle agglomerations or completely impede fiber formation due to nozzle clogging. In centrifugal spinning, the fiber diameter can be reduced by modifying the properties of the solution, such as the viscosity and solvent vapor pressure, and also the spinneret rotational speed [83]. High vapor pressure solvents can lead to higher viscosities during the formation of the polymer jet preceding the fiber formation. Thus, reducing the viscosity can lead to smaller fiber diameters. Fibers with small diameters can also be formed utilizing lower vapor pressure solvents [84,85]. In fact, the solvent evaporation and spinneret rotational speed play an important role in determining the fiber morphology and diameter [84]. For materials used to produce carbon-fiber anodes via centrifugal spinning, high vapor pressure solvents such as methanol, acetone and ethanol are frequently utilized, leading to larger average diameters. However, solutions prepared with low vapor pressure solvents such as water can produce smaller fiber diameters. For example, PEO and PVA fiber, prepared by centrifugal spinning showed an average diameter of 500 and 304 nm, respectively [32,86,87,88]. From our perspective, the nano size scale is in the range of 1–100 nm [89]; any size above 100 nm is in the submicron range. In our previous work on the electrospinning of lanthanum titanate oxide/PAN/DMF precursor solutions for fibrous mats for battery separators, it was reported that the electrospun LOT/PAN composite fibers had an average diameter of 250 nm [90]. In general, nanowires, nanotubes, and nanoparticles with 1–20 nm are considered nanomaterials. For battery applications, the volume to surface ratio is an important characteristic to improve the Li-ion diffusion in the electrode and to increase contact area between the fiber-electrode and electrolyte. Thus, the use of the term “nanofiber” in most of the work published on electrospinning or centrifugal spinning is misleading. The average fiber diameter of the composite fibers discussed in this review as anodes in LIBs and SIBs is in the submicron range.

It is worthwhile to mention here that electrospinning is also capable of producing fibers in the sub-micron range [91,27,92]. However, to achieve smaller fiber diameters in electrospinning, lower flow rates need to be selected, which results in a low production rate [91]. For example, when producing electrospun PVA fibers from aqueous solutions, the average diameter of the fibers ranged from 250 nm to 2 μm [93,94].

Aqueous PEO solutions prepared at polymer concentrations ranging from 3 to 7 wt% were also used to produce fibers in electrospinning with diameters between 34 nm (3 wt% PEO) and 450 nm (7 wt% PEO). Similarly, changing the viscoelastic properties of the polymer solution either through the solvent, adding plasticizing agents, or increasing angular speed can further expand the fiber dimeter range of centrifugally spun PEO fibers. Studies on the centrifugal spinning of PEO fibers have shown that, similarly to electrospinning, the fiber diameter was increased with increasing polymer concentration [87]. Moreover, unlike in electrospinning, the nozzle-to-collector distance in centrifugal spinning does not affect the applied drawing forces (centrifugal forces) to the solution or melt during spinning. In fact, the nozzle-to-collector distance is another processing parameter that can control the diameter of centrifugally spun fibers, as observed in Fig. 7.

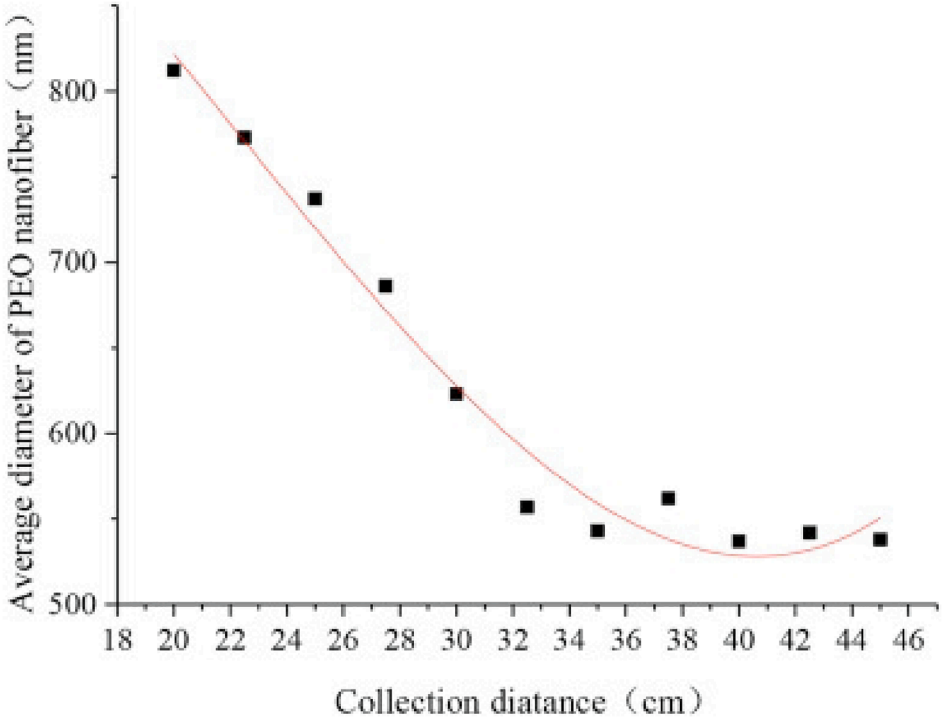

Fig. 7. Average diameter as a function of nozzle-to collector distance (cm) for a 6 wt% PEO solution after Zhang et al. with permission [87].

Recently, our team has successfully produced PEO/Ag composite fibers from aqueous solutions with an average diameter of ~280 nm (Fig. 8). In summary, changing the properties of the polymer solution, either through the amount of solvent being used and/or adding a plasticizing agent/salt to the solution, and increasing the spinneret rotational speed can have vital effects on the diameter and morphology of centrifugally spun fibers.

It is important to note here that the elongation of the polymer jet during the formation of fibers in centrifugal spinning of binary systems (polymer/solvent) can initiate phase separation. When the solution jet is formed and elongation begins, flash vaporization, decompression of the polymer solution, and cooling due to the consumption of heat during vaporization accompany the process [95]. During this process, the polymer jets become thermodynamically unstable and phase separation takes place by forming polymer-rich and solvent-rich phases [95]. Thus, this process can be considered a TIPS phase inversion method. Moreover, evaporation of solutions with solvent mixtures in centrifugal spinning can lead to porous structures due to phase separation. A mechanism that can explain this is that during jet elongation, the solvent with a higher vapor pressure evaporates more rapidly, leaving behind the solvent with a lower vapor pressure. As the higher vapor pressure solvent evaporates, the lower vapor pressure solvent clusters and become the solvent-rich phase that eventually forms pores in the fibers [23]. In the case of a centrifugal spinning polymer solution containing solid nanoparticles, one can assume that if the particles are found in the polymer-rich phase, then this can result in the agglomeration of nanoparticles in the fiber matrix. Similarly, agglomeration could occur if the particles are found in the solvent-rich phase, but in this case, the particles will be placed in the pores, which is beneficial for battery applications to reduce the volume expansion of the electrode. On the other hand, active material agglomeration in the carbon matrix is not beneficial since this structure limits the accessibility of Li^+ to the active material.

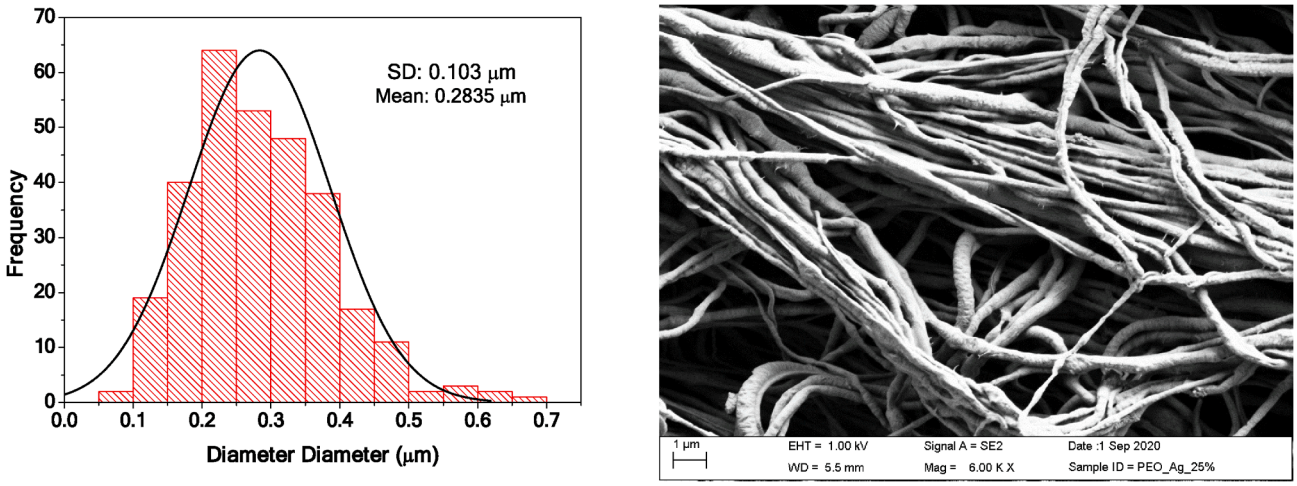

Fig. 8. Histogram, linear distribution, and SEM image of centrifugally spun PEO/Ag composite fibers [Alcoutlabi and coworkers, unpublished data].

3. Centrifugally spun fibers

3.1. Carbon fibers

Carbon fibers can be prepared from different polymer precursor solutions or melts. Solutions made from polymers such as polyacrylonitrile (PAN), polyvinylpyrrolidone (PVP), polyvinyl alcohol (PVA), polyvinylidene fluoride (PVDF), among others [96] have been used as CFs precursors. Currently, 95% of CFs are produced from PAN precursor fibers due to their high carbon yield after carbonization [97,98]. When used in LIBs, carbon-fiber anodes prepared from centrifugally spun PAN precursor fibers delivered a reversible capacity of 297 mAh g^{-1} after 100 cycles at 100 mAg^{-1} [75]. Nevertheless, the high cost of PAN limits the large scale production of carbon-fiber anodes for LIBs [97]. Moreover, dimethylformamide (DMF) is the commonly used solvent for PAN solution, but DMF is toxic and can raise environmental concerns for large scale production of CFs [49]. As a result, economical, environmentally friendly, and water-soluble polymers such as PVP and PVA are becoming increasingly popular alternatives for the preparation of CFs [49,99]. However, these polymer alternatives have relatively lower carbon yields and in the case of PVP, severe shrinkage is observed after carbonization [99,100]. Nonetheless, our group has successfully produced flexible CFs with reduced volume shrinkage during carbonization, from aqueous PVP precursor solutions via centrifugal spinning and a novel three-step heat treatment [101]. This thermal treatment enabled the production of flexible CFs at higher temperatures than that used in previous work [99,102,103]. These CFs were used directly as anodes in half-cell Li-ion batteries and delivered a capacity of 275 mAh g^{-1} after 100 cycles at a current density of 100 mAg^{-1} [101]. Results on CFs prepared from electrospun PAN precursor fibers and subsequent thermal treatment showed that carbonization temperature plays a central role in increasing conductivity and carbon yield relative to residual elements after pyrolyzing PAN (C_3H_3N) [104]. Achieving such high conductivities enables stand-alone CF anodes to function properly without the addition of conductive fillers or a current collector.

3.2. Centrifugally spun composite fibers for LIB anodes

Centrifugally spun composite fibers have been recently used as anode materials for LIBs and SIBs. The electrochemical performance of the composite anodes varies depending on the amount of active material embedded in the carbon fiber matrix, the properties of the polymer precursor solution, and processing parameters. In the following subsections, we summarize and discuss results on composite-fibers prepared by CS and subsequent thermal treatment for use as anodes in LIBs.

3.2.1. Alloying based materials

Common characteristics of alloying based materials include their high theoretical capacity accompanied by a large volume change during charge/discharge cycles, which can lead to anode fracture and crumbling. To retain the higher capacity offered by alloying based materials, volume buffering structures need to be implemented in centrifugally spun fibers. In general, two main methods have successfully achieved high capacities for highly expandable materials. One approach involves introducing pores in the fibers where the particles are located. This clearance between the particles and fibers is filled by the expansion of the nanoparticles after lithiation, thus decreasing the overall volume change of the anode [105–108]. The other method involves constraining the volume change of the particles by encapsulating them in a carbon matrix [49,109,110]. These approaches could be implemented in the future to improve the electrochemical performance of centrifugally spun composite-fiber anodes for LIBs. Table 1 illustrates a list of alloy-based materials used in the preparation of composite-fiber anodes via CS for LIBs. Each of these materials is discussed in the following subsections.

3.2.1.1. Si/C. Silicon is perhaps the most promising material for use as an anode in LIBs because it can accommodate up to $4.4Li^+$ per Si atom via its alloying mechanism, which enables the Si anode to achieve its high theoretical capacity of 4200 mAh g^{-1} at a low alloying/dealloying potential [114]. The low potential can result in a higher open voltage window, leading to a higher energy density battery. However, the low potential also leads to the formation of a large SEI layer because of the LUMO in commercial organic electrolytes. Furthermore, the large SEI layer can also lead to irregular exfoliation of the Li counter electrode, leading to the formation of dendrites that can cause electronic disconnection and short circuits [115]. Despite these challenges, harnessing the high capacity of silicon is the target of many researchers. For this reason, centrifugally spun Si/C CFs have been prepared using water-soluble PVA as the polymer precursor [111,116]. As expected, the large volume change of Si can cause a significant capacity fading after the first cycle due to repeated breaking and formation of the SEI layer [105,117]. Nonetheless, the discharge capacity increased from 625 mAh g^{-1} to 758 mAh g^{-1} from the 20th cycle to the 50th cycle at a current density of 100 mA g^{-1} [111]. Also, control samples of PVA-derived CFs were prepared for comparison. The carbon-fiber anode maintained a capacity of ~178 after 50 cycles at 100 mAg^{-1} [111].

3.2.1.2. Sn/C. Tin has a theoretical capacity of 993 mAh g^{-1} [118] however, Sn suffers from a large volume change during charge/discharge cycles, resulting in anode cracking and pulverization [118]. To reduce volume expansion, Sn nanoparticles (60–80 nm) and microparticles (150 nm) embedded in centrifugally spun porous PAN CFs were prepared to investigate the impact of the Sn particle size on the electrochemical performance of Sn/C composite fibers [75]. Composite fibers containing Sn nanoparticles and microparticles showed capacities of 715 and 724 mAh g^{-1}, respectively, after 50 cycles at a current density of 100 mA g^{-1} [75]. One of the main advantages of smaller particles includes their higher surface area, which allows for more

Table 1
Alloying based materials used in the preparation of composite carbon fibers via centrifugal spinning for use as anodes in LIBs.

Composite fiber anode material	Polymer precursor(s), additive(s), and solvent(s)	Spinning conditions	Stabilization and carbonization	Electrochemical performance at 100 mAh g^{-1}	Reference
Si/C	14% PVA/DI water + 19% Si/DI water	5000 rpm for 5 min,	Partially carbonized by acid treatment followed by carbonization at 800 °C for 30 min.	758 mAh g^{-1} after 50 cycles	[111]
Sn/C	[12% PAN (15% Sn)]/ DMF	8000 rpm	Stabilized at 280 °C for 5 hrs. and carbonized at 800 °C for 2 hrs.	715 and 724 mAh g^{-1} after 50 cycles for nano and micro particles, respectively	[75]
Sn/C	[12% PAN (15% Sn)]/ DMF	8000 rpm	Stabilized at 280 °C for 5 hrs. and carbonized at 800 °C for 2 hrs.	675 mAh g^{-1} after 100 cycles with a ten minutes rest between each discharge cycle.	[112]
Sb/C	[4 g PVB + 5 g SbCl3]/ 40.0 mL methanol	–	Carbonized at 600 °C for 2 hrs	315.9 mAh g^{-1} after 100 cycles	[113]
Sb/C	[4 g PVB + 4 g SbCl3]/ 40.0 mL methanol	–	Carbonized at 600 °C for 2 hrs	254.4 mAh g^{-1} after 100 cycles	[113]
Sb/C	[4 g PVB + 6 g SbCl3]/ 40.0 mL methanol	–	Carbonized at 600 °C for 2 hrs	131.1 mAh g^{-1} after 100 cycles	[113]

alloying/dealloying sites for Li-ions. However, no significant difference in the capacity was observed between Sn-nanoparticles/C and Sn-microparticles/C composite fibers after 40 cycles. This could be attributed to the arbitrary dispersion of particles within the porous fiber matrix and the agglomeration of Sn nanoparticles during centrifugal spinning.

3.2.1.3. Sb/C. Antimony has been widely used with carbon as a nanocomposite anode for LIBs because of its relatively high theoretical capacity of 660 mAh g^{-1} [113]. Recently, Sb/C composite fibers were prepared by centrifugal spinning followed by a heat treatment. Three different precursors of $SbCl_3$/PVB with weight ratios of 4:4, 5:4, and 6:4, labeled Sb4, Sb5, and Sb6, respectively, were used to prepare anodes [113]. In this case, the Sb/C composite fibers were used as an active material to prepare a slurry coated onto copper foil with a ratio of 8:1:1 for the active material, carbon black, and PVDF binders, respectively. By using slurry-based electrodes for Li-ion half cells, the authors were able to reduce the overall thickness of the anode while improving the mechanical properties by the addition of the binder and provided a continuous pathway for electron transfer through the short fibers. Moreover, the addition of carbon black further increased the conductivity of the Sb/C composite-fiber electrode. The results presented for all three anodes included charge/discharge curves, cycle performance, rate performance, and electrochemical impedance. The Sb4, Sb5, and Sb6 anodes delivered discharge capacities of 254, 316, and 131 mAh g^{-1} after 100 cycles, respectively [113]. A general observation with Sb/C composite fibers is that an increase in Sb loading (wt.%) enhanced the Li^+ storage capacity in the anode, but it negatively affected the cycle performance due to the aggregation of Sb nanoparticles, which led to high volume change and crumbling of the active material [113]. This trend can be observed in the cycle performance of these materials, as shown in Fig. 9.

3.2.2. Carbon/Metal-Oxide composites

Metal oxides can host Li-ions either by alloying, intercalation, or conversion. In some cases, metal-oxides exhibit a two-step reaction in which a conversion reaction first forms a lithium oxide layer, followed by the alloying mechanism (alloying or intercalation) of the transition metal. In this review, metal oxides comprise the widest variety of materials. Table 2 shows a summary of the different materials prepared via CS and their electrochemical performance.

3.2.2.1. Cu_2O/C. Copper (I) oxide (Cu_2O) and copper (II) oxide (CuO) are attractive materials for use as anodes in LIBs due to their redox catalyst activity, nontoxicity, affordability, natural abundance, and high theoretical capacity (674 mAh g^{-1}) [33,124]. CuO/C composite-fiber anodes for LIBs were prepared recently using the centrifugal spinning followed by a heat treatment [119]. The CuO/PAN solution precursor was prepared from 15 wt% CuO in a 12 wt% PAN/DMF solution. The CuO/C composite anode delivered a capacity of ~180 mAh g^{-1} after 100 cycles [119]. The centrifugally spun composite fibers show a high irreversible capacity at the first cycle, which was due to SEI formation and the high surface area of fibers. The low capacity of the CuO/C composite anode after 100 cycles in part originated from the low content of active material (CuO) in the carbon-fiber matrix. Unfortunately, at higher concentrations, the CS process did not yield fibers. Increasing the amount of active material resulted in a high viscosity solution that was difficult to process by CS. The same processing difficulties can be encountered in electrospinning.

3.2.2.2. MoO_2/C. Molybdenum Oxide (MoO_2) is an attractive metal oxide for anode preparation because of its low electrical resistivity (8.8 × 10^{-5} Ω cm) and high theoretical capacity (838 mAh g^{-1}) [125]. However, one of the biggest challenges for MoO_2 anodes is obtaining large specific capacities at higher current densities [125]. Recently, MoO_2/C composite fibers were prepared by the centrifugal spinning of MoO_2 precursor (Ammonium molybdate) at different concentrations of 40, 50, 60, 70, and 80 wt% in 15 wt% PAN/DMF solutions. Fig. 10a through d show the cycle performance results for the 50, 60, 70, and 80 wt%. Active material in the PAN/MoO_2 precursor fibers. Looking at the different charge/discharge plots, one can identify that anodes made from the 70 and 80 wt% active material delivered the highest specific capacities. This can be attributed to the larger amount of active material exposed to lithiation. However, structural instabilities induced by strain in the anode lead to capacity fading and/or poor performance. Also, a higher active material loading did not necessarily yield higher specific discharge capacities. The MoO_2/C composite-fiber anodes with 50 and 60 wt% active material in the PAN/MoO_2 precursor, Fig. 10a and b, respectively, illustrate this claim because the 50 wt% delivered more stable and higher capacities despite its lower loading of active material. Thus, it can be concluded that implementing techniques to better distribute the active material within the fibers can be just as effective, if not more effective, than simply increasing the amount of active material to improve the anode capacity.

3.2.2.3. Fe_3O_4/C. Magnetite (Fe_3O_4) is considered a potential anode material for LIBs owing to its low cost, low toxicity, and high theoretical capacity (~924 mAh g^{-1}) [96]. However, Fe_3O_4 exhibits limited ion

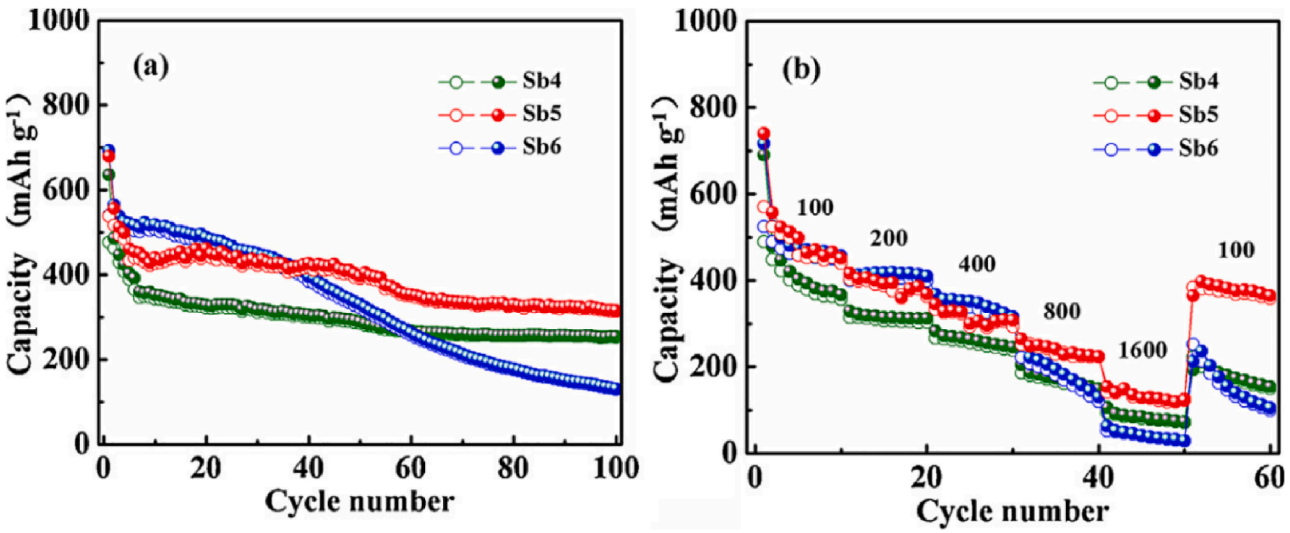

Fig. 9. a) Cycle performance, and b) rate performance for Sb4, Sb5, and Sb6. After Lv et al. [113] with permission.

Table 2
Transition metal oxides used in the preparation of composite carbon fibers via centrifugal spinning for use as anodes in LIBs.

Composite fiber anode material	Polymer precursor(s), additive(s), and solvent(s)	Spinning conditions	Stabilization and carbonization	Electrochemical performance at 100 mA g^{-1}	Reference
CuO/C	[12 wt% PAN (15 wt% CuO)]/DMF	7,000 rpm	Stabilized at 280 °C for 5 hrs and carbonized at 700 °C for 2 hrs	~ 160 mAh g^{-1} after 100 cycles	[119]
MoO_2/C	[12 wt% PAN (50, 60, 70, and 80 wt%. MoO_2)]/DMF	6,800 rpm	Stabilized at 280 °C for 5 hrs and carbonized at 700 °C for 2 hrs	629, 575, 597, 710 mAh g^{-1} during the first cycle, respectively.	[120]
Fe3O4/C	[12 wt% PAN (15 wt% FeACAC)]/DMF	7,000 rpm	Stabilized at 280 °C for 4 hrs and carbonized at 600 °C for 6 hrs	300 mAh g^{-1} after 100 cycles	[96]
TiO_2/C	[15 wt% PVP (17:4 wt ratio Titanium/PVP)]/[10:1 wt ratio ethanol/acetic acid	7,000 rpm	Stabilized at 280 °C for 5 hrs and carbonized at 550 °C for 5 hrs	228.9 mAh g^{-1} after 100 cycles	[102]
TiO_2/C	(5 g PVP + 3 g TBOT)/[40 mL methanol]	20,000 to 30,000 rpm (0.1 mm diameter aperture)	20,000 to 30,000 rpm (0.1 mm diameter aperture)	150 mAh g^{-1} after 200 cycles.	[121]
α Fe_3O_4/C	[28 wt% PVP (2 g $Fe(NO_3)_39H_2H$)]/H_2O [12 wt% PAN]/DMF	7000–7500 rpm	PVP - Stabilization at 600 °C for 1 hr. PAN - Stabilized at 240 °C for 30 mins. and carbonized at 800 °C for 1 hr	505 mAh g^{-1} after 100 cycles	[122]
α-Fe_2O_3/TiO_2/C	[15 wt% PVP (1 g titanium (IV) butoxide, 1.5 g iron (III) acetylacetonate)]/ethanol/acetic acid (10:1)	7000 rpm	PVP – Stabilization at 200 C for 2 h carbonization at 550° C for 5 h.	340 mAh g^{-1} after 100 cycles.	[123]
Fe_3O_4/Fe_3C/C	(5 g PVP + 3 g $Fe(acac)_3$)/[40 mL methanol]	20,000 to 30,000 rpm (0.1 mm diameter aperture)	Dried at 60 °C for 12 h. Pre-oxidized at 300 °C for 2 h. carbonization at 600 °C for 2 h.	400 mAh g^{-1} after 200 cycles.	[121]
Fe_3O_4/Fe_3C/TiO_2/C	5 g PVP + 3 g $Fe(acac)_3$)/[/[40 mL methanol + 3 mL TBOT]	20,000 to 30,000 rpm (0.1 mm diameter aperture)	Dried at 60 °C for 12 h. Pre-oxidized at 300 °C for 2 h. carbonization at 600 °C for 2 h.	700 mAh g^{-1} after 400 cycles	[121]
NiO/C	[12 wt% PAN (15% NiO)]/DMF	7,000 rpm	Stabilized at 280 °C for 5 hrs and carbonized at 700 °C for 2 hrs	~ 200 mAh g^{-1} after 100 cycles	[119]
SnO_2/C	[12 wt% PAN (15% SnO2)]/DMF	7,000 rpm	Stabilized at 280 °C for 5 hrs and carbonized at 700 °C for 2 hrs	211 mAh/g after 50 cycles	[119]
SnO_2/NiO/C	[12 wt% PAN (15% Sn 2-ethylhexanoate, 10% Nickel (II) acetate tetrahydrate)]/DMF	8000 rpm	Stabilized at 280 °C for 5 hrs and carbonized at 800 °C for 2 hrs	633 mAh/g after 100 cycles with a ten minutes rest between each discharge cycle.	[112]
ZnO/C	[12 wt% PAN (15 wt% ZnO)]/DMF	7,000 rpm	Stabilized at 280 °C for 5 hrs and carbonized at 700 °C for 2 hrs	~ 235 mAh/g after 80 cycles	[119]

diffusion and loss in specific capacity caused by its high volume change after repeated charge/discharge cycles [114]. One method that has been widely used to reduce the volume change is to disperse Fe_3O_4 nanoparticles in a carbon-fiber matrix [26]. For this reason, Fe_3O_4/C composite fibers have been prepared by the centrifugal spinning of iron (III) acetate homogenized in a PAN/DMF solution. Then, the fibers were prepared and subsequently stabilized at 250 °C in air, and carbonized at 600 °C under an argon environment. The Fe_3O_4/C composite-fiber anode delivered a reversible capacity of 328 mAh g^{-1} after 100 cycles at a constant current density of 100 mAg^{-1}. The amount of Fe_3O_4 (active material) in the precursor solution was 15 wt%. Thus, a low capacity was observed after 100 cycles [96]. A high loss in capacity after the first cycle caused by the high surface area and large thickness of the fiber anodes was observed, indicating that a thick SEI layer was formed.

In a similar study, CS was employed to produce hollow α-Fe_3O_4/C composite fibers for use as anodes in LIBs [122]. α-Fe_3O_4 has high theoretical capacity of 1004 mAh g^{-1}, low toxicity, and is abundant [122]. In contrast to previous methodologies, the active material was not introduced in the solution before centrifugal spinning. Instead, hollow PAN fibers were first produced by centrifugal spinning. Then, these fibers were immersed in a solution prepared from ground heat-treated α-Fe_3O_4/PVP fibers and ethanol. The soaked fibers were then dried and carbonized. Additionally, pristine CFs (PAN/DMF) were prepared using the same carbonization process to compare the electrochemical performance of the CFs coated with α-Fe_3O_4/PVP precursor solution with that of the pristine CF (control). After the second cycle, both the CFs and α-Fe_3O_4/C composite fibers retained a relatively constant capacity of 200 and 505 mA g^{-1} [122]. For these anodes, the SEI layer completely formed after the first cycle and no further Li^+ were consumed if the following cycles leading to stable capacities. Moreover, these fibers provided excellent ion accessibility during lithiation/delithiation, since they did not suffer a significant loss in capacity at higher current densities and regained their capacity when cycled back at lower current densities during the rate performance testing.

3.2.2.4. TiO_2/C. Titanium dioxide (TiO_2) can be found in polymorphic states such as anatase, rutile, brookite, and TiO_2-II (bronze). Among the various configurations, the anatase phase has been widely used in LIBs because it is the most electroactive host for Li^+ intercalation [46]. Moreover, TiO_2 is an attractive anode material due to its environmental friendliness, low cost, abundancy, low volume expansion (3–4%), and moderate theoretical capacity (335 mAh g^{-1}) [126,102]. Although the theoretical capacity of TiO_2 is lower than that of graphite (372 mAh g^{-1}), TiO_2 possesses a higher operating potential (<0.8 V vs Li/Li^+) [31,127]. This is beneficial because it is closer to the LUMO of commercial organic electrolytes DMC/DEC (1.2 eV) [31]. For these reasons, hollow and non-hollow fibers with anatase TiO_2 filler were prepared by CS. Fig. 11 shows the cycle performance plots of the hollow and non-hollow TiO_2/C composite fibers. It is observed that the capacity of the hollow fibers is higher than that for the non-hollow fibers and increases with increasing cycle number. This could be attributed to the porous and hollow structure, which allows the TiO_2 to accommodate more Li^+ within the structure owing to the extra access of electrolyte to the active material after prolonged charge/discharge cycles.

3.2.2.5. α-Fe_2O_3/TiO_2/C. As mentioned in Section 3.2.2.3, α-Fe_3O_4 has a high theoretical capacity of 1004 mAh g^{-1} [122] but it also suffers from loss in specific capacity due to the high volume change after prolonged charge/discharge cycles [114]. On the other hand, titanium dioxide has a low volume expansion (3–4%) and moderate theoretical capacity (335 mAh g^{-1}) [126,102]. Thus, α-Fe_2O_3/TiO_2/C composite fibers prepared through CS were used as flexible binder-free anodes in

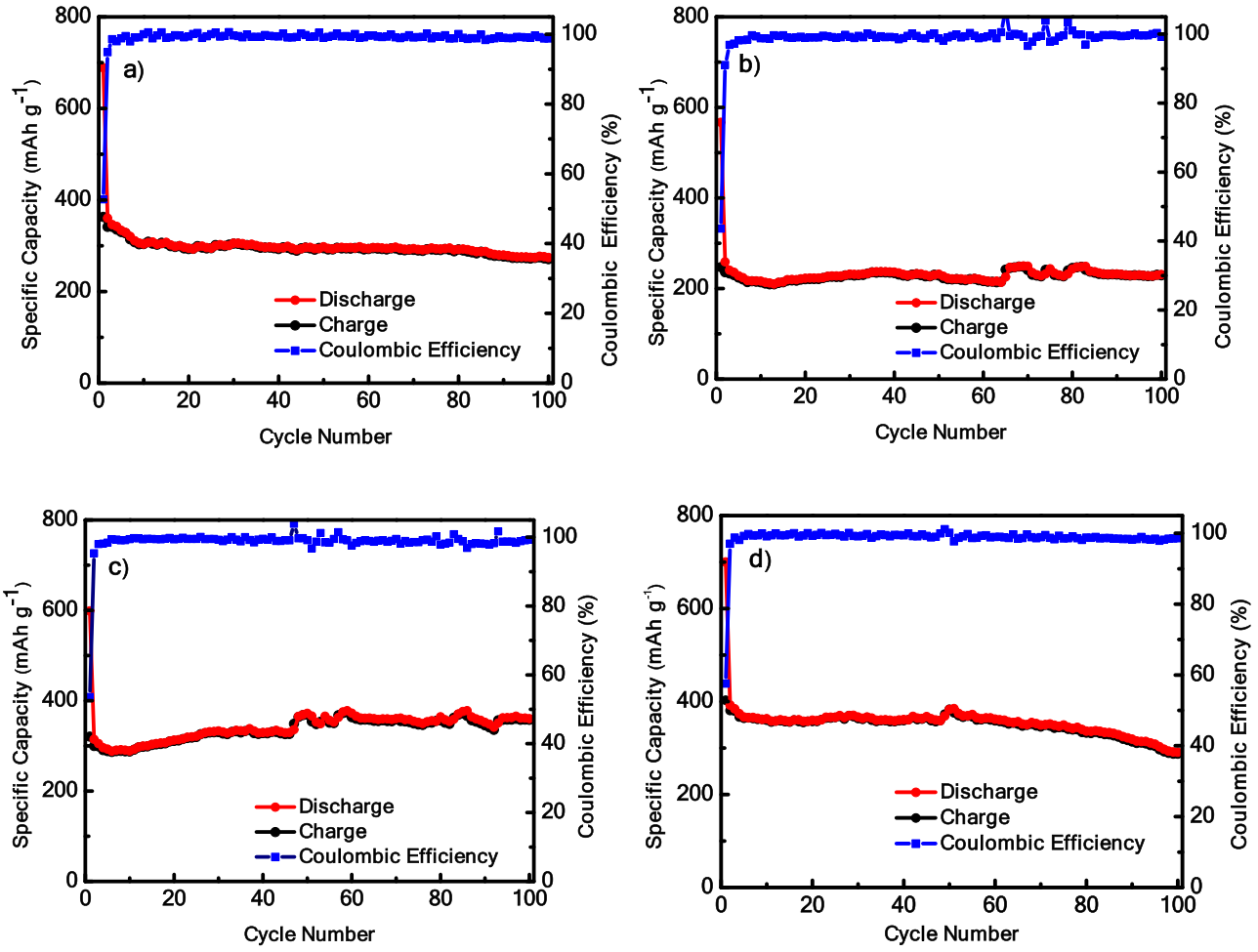

Fig. 10. Charge/discharge and cycle performance graphs for a) 50%, b) 60%, c) 70%, and d) 80% active material (MoO_2). After Valdez et al. [120] with permission.

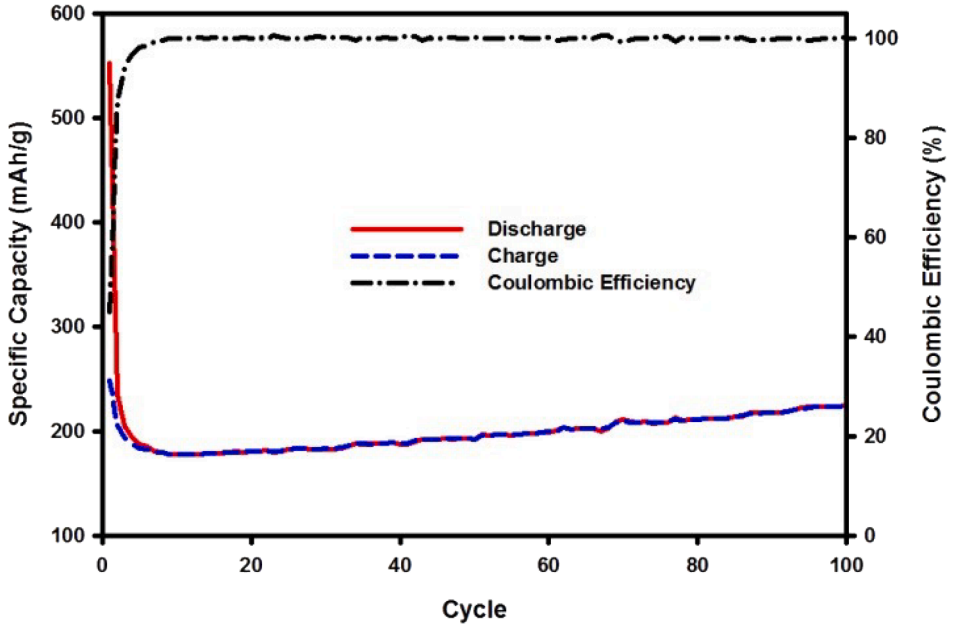

Fig. 11. Cycle performances for a) non-hollow and, b) hollow TiO_2/C composite fibers. After Zuniga et al. [102] with permission.

LIBs with the intent to buffer the volumetric strain of α-Fe_2O_3 by adding TiO_2, while simultaneously maintaining a high specific capacity of α-Fe_2O_3 [123]. Moreover, TiO_2/C and α-Fe_2O_3/C composite-fiber electrodes were also prepared to compare their performance with that of the ternary α-Fe_2O_3/TiO_2/C composite-fiber anode. After 100 cycles at 100 mA g^{-1}, the TiO_2/C and α-Fe_2O_3/C composite-fiber anodes showed a specific capacity of 61 mAh g^{-1} and 121 mAh g^{-1}, respectively. Under the same conditions, the α-Fe_2O_3/TiO_2/carbon composite anodes showed a final capacity of 340 mAh g^{-1} [123]. Based on the cycle performance results shown in Fig. 12, one can identify the improved performance of the ternary α-Fe_2O_3/TiO_2/C composite-fiber anode. This is expected since the superior structural stability upon cycling of TiO_2 and the higher capacity of Fe_2O_3 play their respective roles during the lithiation/delithiation processes.

3.2.2.6. Fe_3O_4/Fe_3C/TiO_2/C. This complex composite material aims to achieve a high capacity with the addition of Fe_3O_4, leverage the catalytic conversion reaction of Fe_3C to stabilize the passivation layer formation (SEI), and lower strain through the addition of TiO_2 in the carbon fiber matrix. Fe_3O_4/Fe_3C/TiO_2/C composite CFs, termed FTC, were prepared and to compare their performance, Fe_3O_4/Fe_3C/C composite fibers, termed FC, and TiO_2/C composite fibers, termed as TC, were also fabricated using CS and the same heat treatment. These three composite CFs, however, were not used as binder-free working electrodes. They were prepared as slurries with proportions of 8:1:1 for active material: carbon black: PVDF using N-methyl-2-pyrrolidinome (NMP) as the solvent. By implementing slurry-based electrodes instead of the stand-alone composite fibers as the working electrodes, the authors were able to reduce the total thickness of the anode, which in turn reduced the SEI layer thickness, improved the conductivity of the anode with the addition of carbon black, and improved the mechanical properties (i.e., strength) with the introduction of the binder. All three working electrodes were tested at a current density of 100 mAh g^{-1} and their cycle performance results are shown in Fig. 13. It can be seen in Fig. 13 that the FTC anode outperforms the TC and FC electrodes. After 200 cycles, the FC and TC anodes delivered a discharge capacity of 383 mAh g^{-1} and 140 mAh g^{-1}, respectively [121]. In comparison, the FTC working electrode delivered 700 mAh g^{-1} after 200 cycles and slightly increased to 702 mAh g^{-1} after 400 cycles [121]. Moreover, the FTC anodes were also capable of delivering 130 mAh g^{-1} after 350 cycles at a current density of 1000 mA g^{-1}. This prolonged life cycle and ability to deliver relatively high discharge capacities at high current densities can be attributed to the complex compound used to prepare the anode, the nanostructure of the fibers which facilitated electron pathways, and the addition of conductive agents such as carbon black.

3.2.2.7. NiO/C. Nickel (II) oxide (NiO), in particular, is an attractive material because of its high theoretical capacity (718 mAh g^{-1}). However, NiO also faces challenges such as large volume change and low electronic conductivity [128,129]. As a transition-metal, Ni is inert towards Li [50]. However, Ni functions as a catalyst in the conversion of NiO into Ni nanoparticles and the conversion of Li into Li_2O. The ability of oxygen to reversibly react with Li and Ni allows the anode to partially reverse the formation of the SEI layer and leads to relatively high reversible capacities [50]. Because of the catalytic reaction of Ni, NiO displays excellent reversible capacity, capacity retention, and excellent rate performance at specific NiO contents in composite carbon binder-free anodes [130,131]. For these reasons, centrifugally spun NiO/PAN fibers were prepared, calcinated, and used directly as binder-free anodes in Li-ion half-cells. Cycle performance tests were performed over a voltage window of 0.05 – 3.00 V and a current density of 100 mAh g^{-1} [119]. The NiO/C composite-fiber anode delivered a capacity of 250 mAh g^{-1} after 100 cycles at 100 mA g^{-1}. After the formation of SEI in the first discharge cycle, a steady capacity fading was observed. This can be attributed to the formation of the solid interface electrolyte SEI caused by the high surface area of the NiO/C composite fibers. It can be deduced that the reversible decomposition of Li_2O could not take place if the SEI layer separated the active material from incoming Li-ions. This issue could be solved by implementing a structure that increases pathways for ion transport between the SEI and the active material. For example, NiO nanoparticles have been also embedded in porous carbon fibers prepared by electrospinning and prepared into a slurry for LIB anodes. In that work, the NiO/C composite anode was capable of delivering 638 mAh g^{-1} after 50 cycles at a current density of 40 mA g^{-1} [128]. Moreover, the NiO/C composite anode delivered a reversible capacity of 696 mAh g^{-1} at 471 mA g^{-1}, which was higher than that of commercial NiO [128]. These results further underscore the benefits of the porous structure that can play a central role in the electrochemical performance

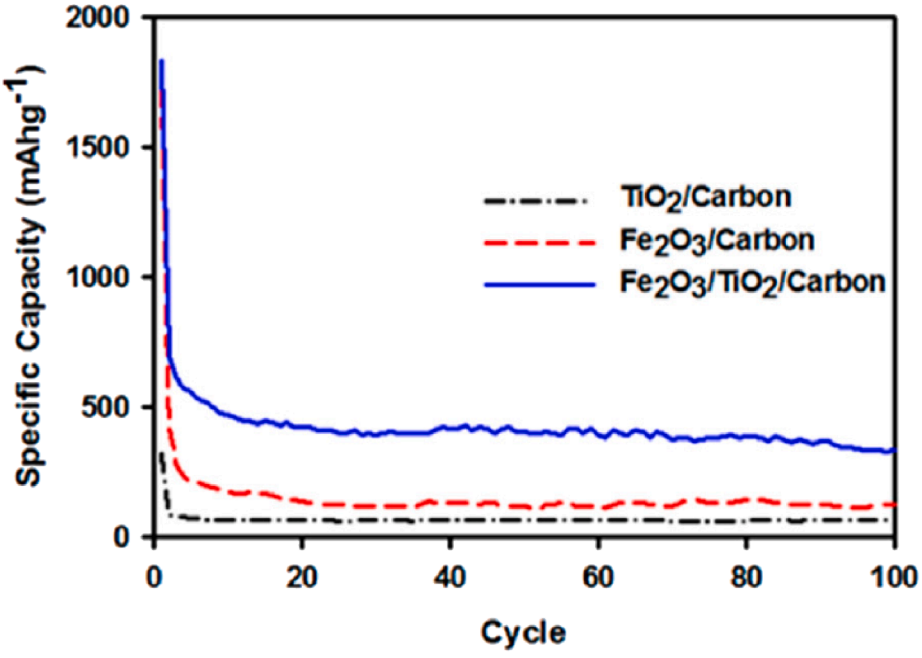

Fig. 12. Cycle performance for α-Fe_2O_3/TiO_2/carbon, TiO_2/C, and α-Fe_2O_3/C composite binder-free anodes at 100 mAg^{-1}. After Zuniga et al. [123] with permission.

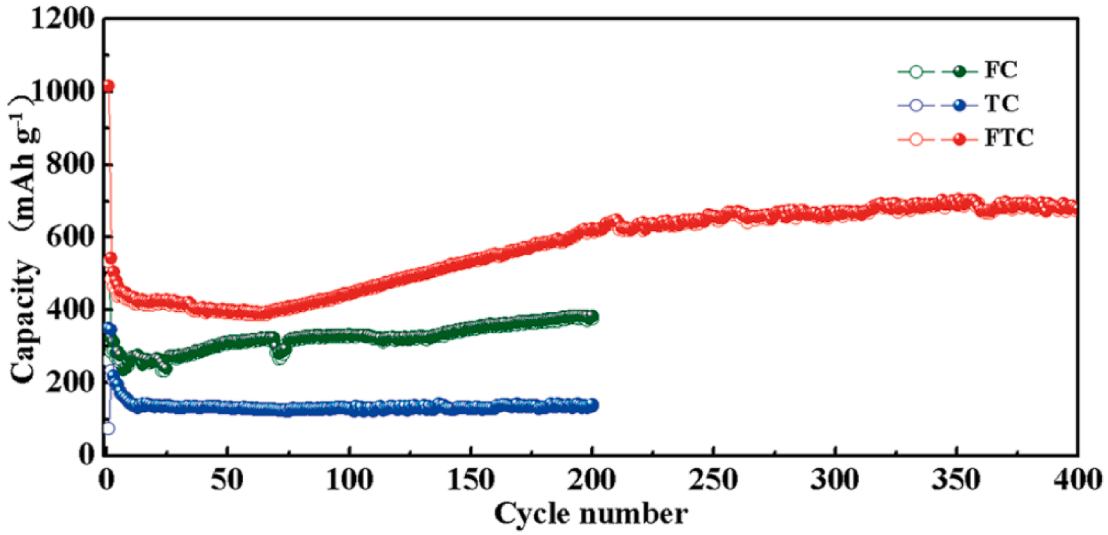

Fig. 13. Cycle performance for the FC, TC, and FTC working electrodes at a 100 mA g^{-1} current density. After Lyu et al. [121] with permission.

of metal oxide/C composite anodes.

3.2.2.8. SnO_2/C. Tin oxide is an alloying-based transition metal oxide material with a high theoretical capacity of (~992 mAh/g) [132]. SnO_2/C composite fibers have been recently fabricated by CS and subsequent heat treatment. After heat treatment, the SnO_2/C composite fibers were directly used as an anode material in LIBs [119]. The SnO_2/C composite-fiber anode delivered a specific capacity of 211 mAh g^{-1} after 50 cycles at 100 mA g^{-1} [119]. After the formation of the SEI layer, a relatively small capacity fading took place thereafter. This can be attributed to the early exhaustion of oxygen in the formation of LiO leading to the stable alloying dealloying reaction of Sn.

3.2.2.9. SnO_2/NiO/C. To achieve higher capacities and increase the reversible capacity, SnO_2/NiO/C composite fibers were prepared via CS and subsequent heat treatment [112]. The SnO_2/NiO/C composite fiber anodes were produced with a "hair-like" structure [112]. Besides, SnO_2/C composite fibers were fabricated to compare their performance with the ternary SnO_2/NiO/C composite-fiber anode. The capacity of SnO_2/C and SnO_2/NiO/C composite electrodes, after 100 charge/discharge cycles at a current density of 100 mAh g^{-1}, were 675 mA g^{-1} and 633 mA g^{-1}, respectively [112]. The cycle performance of the control SnO_2/C and SnO_2/NiO/C composite anodes is shown in Fig. 14. In part, the higher capacity delivered by the SnO_2/C can be attributed to its porous structure, whereas the SnO_2/NiO/C composite fibers had a "hair-like" structure. Moreover, since a portion of the total active material in the solution was substituted by NiO instead of pure Sn, the overall capacity of the composite anode can be expected to be lower due to the lower theoretical capacity of NiO. Nonetheless, the addition of this metal oxide could prolong the battery life while maintaining a higher reversible capacity. This hypothesis could be corroborated if the anodes are cycled for a higher number of cycles. In Fig. 14, it can already be seen that the difference in specific capacities between the anodes is decreasing as the cycles increase.

3.2.2.10. ZnO/C. Despite its low cost, high abundance, and moderate

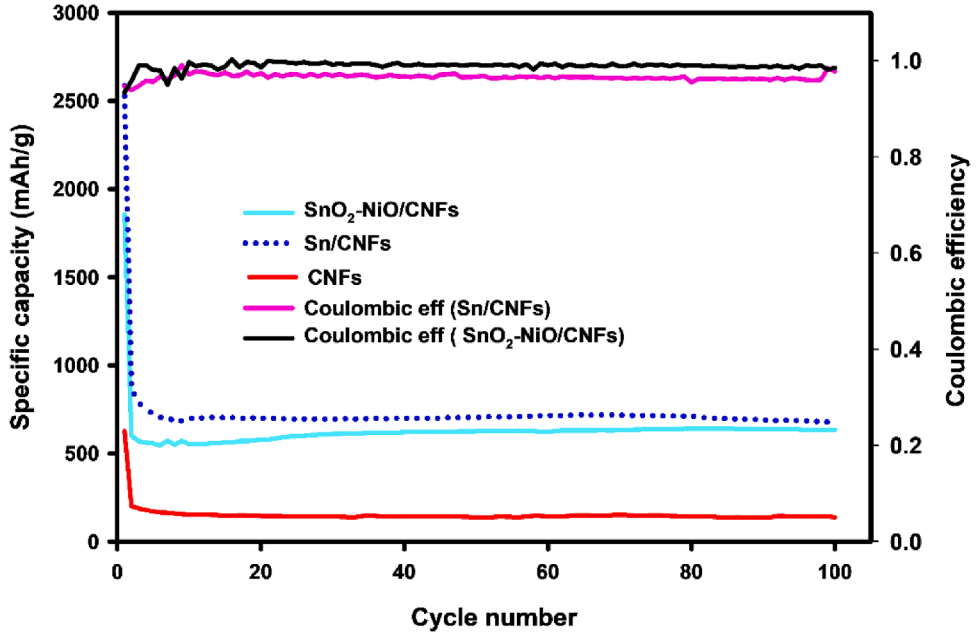

Fig. 14. Cycle performance for PAN-based CFs, of SnO_2/C, and SnO_2/NiO/C. After Agubra et al. [112] with permission.

specific capacity (410 mAh g^{-1}), large volume changes have negatively impacted the electrochemical performance of ZnO [133]. Nonetheless, this material is capable of reversibly forming Li_2O, which can be related to its post-transition metal oxide properties [133,134]. Although early in its research development, there has been a study on centrifugally spun ZnO CFs. Results obtained on Li-ion half-cells showed that the Zn/O composite-fiber anode delivered a capacity of ~225 mAh g^{-1} at a current density of 100 mAh g^{-1} within a voltage window of 0.05 and 3.0 V [119]. The results show a capacity fading with increasing cycle number caused by the volume change of the ZnO/C composite anode. Moreover, a high loss in capacity at the first cycle was observed, which is in agreement with prior results [135]. In a similar work, porous ternary NiO/ZnO/C composite fibers were prepared by electrospinning and subsequent heat treatment. These binder-free anodes showed a significant improvement in a specific capacity of 949 mAh g^{-1} at a current rate of 200 mA g^{-1} after 120 cycles and 707 mAh g^{-1} at a current density of 3200 mA g^{-1} [134]. Thus, these electrospun anodes were able to deliver high specific capacities at high current densities. Fast charge/discharge rates are particularly sought by the EV market, and the anode is one of the main bottlenecks due to the anodes sluggish lithiation/delithiation kinematics [135]. The implementation of ternary composite anodes including ZnO and a porous structure of CS fibers remains to be investigated. This is a potential opportunity to achieve a high production rate of binder-free anodes capable of delivering high specific capacities at high current rates.

3.2.3. Carbon/metal-sulfides composites

There are only two metal sulfide materials utilized in the production of composite carbon fibers via centrifugal spinning for battery applications. Table 3 contains the materials discussed in the following subsections.

3.2.3.1. MoS_2/C. Molybdenum disulfide (MoS_2) is a good alternative anode material for LIBs due to its high theoretical capacity of 670 mAh g^{-1} and layered structure, similar to that of graphite, that can host a high number of Li ions. [137]. Moreover, the chemical structure of MoS_2 (S-Mo-S) is kept together by weaker van der Waals forces which facilitate the intercalation and diffusion of Li ions from the MoS_2 structure [138,139]. Nevertheless, MoS_2 faces intrinsic challenges such as structural degradation due to large strains, which lead to capacity fading [140]. One characteristic of MoS_2 is that it undergoes an intercalation mechanism followed by a conversion reaction (Li_2S) upon lithiation, similar to that of some metal oxides [139]. Reactions (4) and (5) represent the intercalation reaction (plateau at ~ 1.1 V vs Li^+/Li) and conversion reaction (plateau at ~ 0.5 V vs Li^+/Li), respectively [139].

$$MoS_2 + xLi^+ + xe^- \rightarrow Li_xMoS_2 \quad (4)$$

$$Li_xMoS_2 + (4-x)Li^+ + (4-x)e^- \rightarrow Li_2S + Mo \quad (5)$$

Nonetheless, the conversion reaction in MoS_2 is not yet fully understood and different interpretations of this process have been reported [139]. Moreover, unlike metal oxides, the conversion reaction between this metal sulfide and compounds in the SEI is not partially reversible [139]. MoS_2/C composite fibers were prepared by centrifugal spinning and used as anode material for LIBs. The precursor solution was prepared by homogenizing 80 wt% MoS_2 in a 12 wt% PAN/DMF solution. These anodes delivered a specific capacity of 335 mAh g^{-1} after 100 cycles at a current density of 100 mA g^{-1} [120]. Multiple MoS_2 nanostructures such as nanosheets, nanoflakes, and nanowires have been implemented in the development of binder-free composite anodes via electrospinning. Similar experiments still need to explore the use of CS to compare the electrochemical performance of centrifugal spun composite fibers to their electrospun counterpart.

3.2.3.2. TiS_2/C. Titanium sulfide has been typically used as a cathode material in LIBs and as an anode in SIBs [141,142]. However, if used as an anode material in LIBs, TiS_2 can exhibit excellent cycling stability, high electronic/ionic conductivity, and a moderate theoretical capacity of 240 mAh g^{-1} [141,143]. Although TiS_2 has a relatively low theoretical capacity, its high conductivity can enhance the electrochemical performance in ternary composite materials when subjected to higher current rates [144]. TiS_2/C fibers have been prepared via CS for use as anodes in LIBs. The composite fibers were prepared by spinning a 12 wt % PAN in DMF and 30 wt% TiS_2 nanoparticle suspension followed by a carbonization process. Nevertheless, during the heat treatment, the TiS_2 nanoparticles turned into TiO_2 nanoparticles with a 2-D layered structure after the oxidation process in air of the TiS_2/PAN precursor fibers before carbonization. The TiO_2/C composite fibers were used directly as anodes in Li-ion half cells and tested under a constant current density of 50 and 100 mAg^{-1}. It was observed that ~50% of the capacity of the TiO_2/C composite anode was lost after the first cycle due to the formation of the SEI layer. Fig. 15 A shows the charge/discharge curves of the TiO_2/C composite fibers at a constant current density of 100 mAg^{-1}, over a potential range of 0.01–3 V. After 100 cycles at 100 mA g^{-1}, the TiO_2/C composite-fiber anode delivered a specific charge capacity of ~260 mAh g^{-1} [136,25]. The TiO_2/C composite fibers were also tested at a 50 mA g^{-1} current density. Fig. 15 B shows the Coulombic efficiency and cycle performance of the TiO_2/C fiber-anode over 100 cycles at a current density of 100 mAg^{-1}. The results show a final specific capacity of 260 $mAhg^{-1}$ after 100 cycles. The subsequent cycles show excellent stability and a high efficiency of ~ 99% as can be seen in Fig. 15B [25].

3.2.4. Discussion on composite carbon fibers for LIBs

Centrifugal spinning (CS) is an alternative manufacturing approach being explored to increase the production rate of composite fibers (CFs) and improve the safety of LIBs manufacturing. Multiple nanostructures such as nanoparticles, quantum dots, nanorods, and nanosheets have been integrated into electrospun composite CFs, since this has been the most commonly adopted method used in laboratory research. Therefore, it is not surprising to find better results on electrospun composite CFs so far. However, there is plenty of room in CS for the implementation of active materials with different nanostructure configurations. In most cases, the capacity of the electrospun anodes is higher due to their smaller average diameter. However, future refined implementation of centrifugal spinning to fabricate fibers could help optimize the surface area of fibers and, in turn, improve the performance of the centrifugally spun fibers to match and exceed the performance of the more widely implemented electrospun fibers. For example, the electrochemical performance of centrifugally spun binder-free anodes can be improved by the fabrication of fibers via architecture structures (porous and hollow fibers) with high surface area or implementing ternary materials. These approaches can not only be implemented for LIB electrodes but also for

Table 3
Transition metal sulfides used in the preparation of composite carbon fibers via centrifugal spinning for used as anodes in LIBs.

Composite Fiber Anode Material	Polymer Precursor(s), Additive(s), and Solvent(s)	Spinning Conditions	Stabilization and Carbonization	Electrochemical Performance	Reference
MoS_2/C	[12 wt% PAN (80 wt% MoS_2)]/DMF	- Not Specified	Stabilized at 155 °C for 75 mins then Stabilized at 280 °C for 75 mins and carbonized at 810 °C for 1 hr	250 mAh g^{-1} after 100 cycles (tested at 100 mA g^{-1})	[120]
TiS_2/C	[12 wt% PAN (wt.% TiS2)]/DMF	Not Specified	Stabilized at 280 °C for 5 hrs and carbonized at 800 °C for 2 hrs	250 mAh g^{-1} after 100 cycles (tested at 50 mA g^{-1})	[136,25]

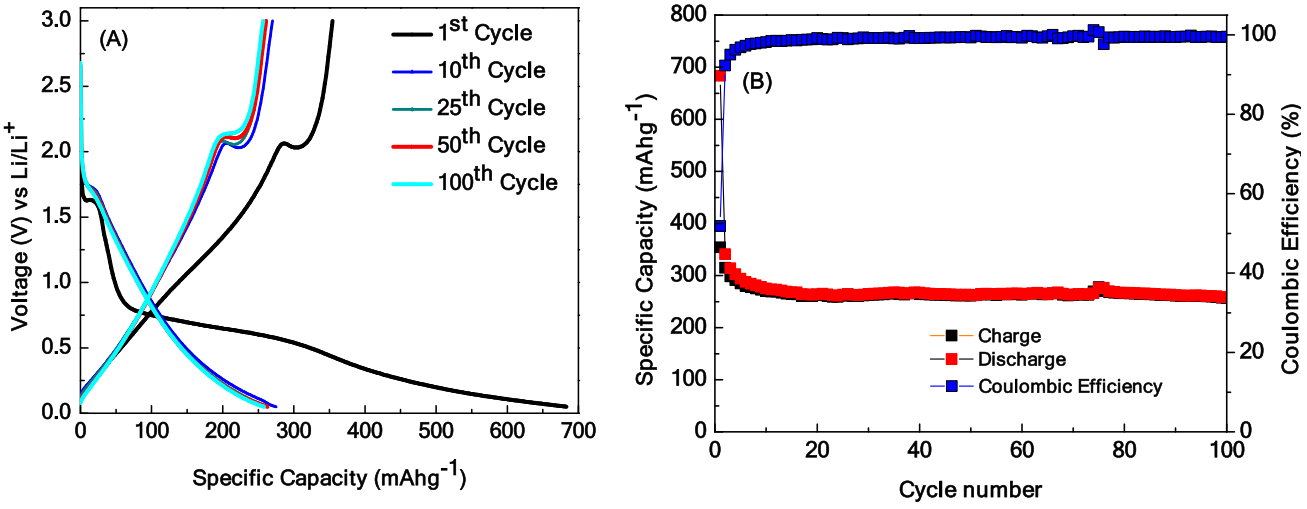

Fig. 15. A) Galvanostatic charge/discharge curves for the TiO_2/C composite-fibers electrode showing the voltage vs specific capacity plots for the 1st, 10th, 25th, 50th, and 100th cycles at current density of 100 mAg^{-1} within a voltage window of 0.05–3.0 V. B) Cycle performance of TiO_2/C composite electrode at 100 mAg^{-1} for 100 cycles. After Lopez et al. [25] with permission.

SIB electrodes. Hence, the following section is focused on the electrochemical performance of CS fibers for SIBs.

3.3. Centrifugally spun composite fibers for SIBs

Due to the increasing demand for electronic devices, EVs, and large scale-stationary energy storage, the relatively deficient amounts of lithium reserves could fail to satisfy the demand for future applications. Hence, alternative materials such as sodium have become a major competitor to lithium due to high natural abundance and low cost [145]. Therefore, research to develop compatible materials for SIBs has seen increasing interest over recent years [145,146,147]. One of the major challenges is the larger ion size. Na^+ has an ion radius of 0.98 Å compared to the smaller Li^+ radius of 0.69 Å [148]. Consequently, Na-ions are less able to intercalate/alloy into the host material. SIBs with a graphitic anode exhibit low capacities of ~35 mAh g^{-1} due to the sluggish intercalation of Na^+ into graphite [149]. CFs prepared by centrifugal spinning and subsequent thermal treatment have been prepared with the objective to alter the structure of the CFs and improve intercalation kinetics between Na^+ and carbon. The produced CFs were used as anodes in Na-ion half-cells and delivered a reversible capacity of 88 mAh g^{-1} after 100 cycles [99]. Even after modifying the structure of the CFs to favor Na^+ intercalation, the carbon-fiber anode delivered less than half the capacity of centrifugally spun CF anode for LIBs. In fact, the smaller ion size of Li^+ was the key parameter that stimulated a higher interest in LIBs when both materials were initially proposed [146]. Among the efforts to overcome the challenges that SIBs face, centrifugally spun composite fibers have been developed for use as anodes in SIBs.

3.3.1. Alloying based materials

There are limited available results on the use of alloying based materials as precursors for centrifugally spun composite-fiber anodes in SIBs. The material composition, additives, heat treatments, and the electrochemical performance of these composite-fiber anodes are listed in Table 4.

3.3.1.1. SnSb/C. Antimony and tin-based anode materials suffer from a large volume change after prolonged charge/discharge cycles. Nonetheless, their high abundance, low toxicity, and high theoretical capacity as a binary alloy (750 mAh g^{-1}) make SbSn a good candidate for SIB anodes [152]. Although Sn and Sb both suffer from a large volume expansion, the SnSb compound is more malleable and its plasticity enables the active material to accommodate more Li^+ and reduce the volume expansion/contraction during charge/discharge cycles [152]. Thus, an SnSb alloy was embedded in a carbon matrix to form centrifugally spun SnSb/C composite microfibers (CMF). These composite fibers were carbon-coated to maintain structural stability during cycling [107]. Moreover, two solutions were prepared with (SnO_2/Sb_2O_5)/PAN ratios of 1:2 and 1:1 denoted as SnSb@CMF-2 and SnSb@CMF-1, respectively [150]. The SnSb@CMF-2 fibers were then carbon-coated and denoted SnSb@CMF-2@C. The SnSb@CMF-1, SnSb@CMF-2, and SnSb@CMF-2@C delivered specific discharge capacities of 359, 345, and 781 mAh g^{-1}, respectively, after 50 cycles at a current density of 100 mA g^{-1} [150]. Fig. 16a and b show the cycle performance and coulombic efficiency for the control and the three composite-fiber anodes. Based on the results, one can easily observe that the effect of carbon coating buffers the volume changes in the SnSb@CMF-2@C and helps maintain a high capacity after 100 cycles. Even though a better

Table 4
Alloying based materials used in the preparation of composite carbon fibers via centrifugal spinning for used as anodes in SIBs.

Composite Fiber Anode Material	Polymer Precursor(s), Additive(s), and Solvent (s)	Spinning Conditions	Stabilization and Carbonization	Electrochemical Performance at 100 mA g^1	Reference
SnSb/C	[15 wt% PAN (50 wt% SnO2/Sb2O5)]/DMF	Not Specified	Stabilized at 250 °C for 2.5 hrs and carbonized at 700 °C for 2 hrs	359 mAh g^1 after 50 cycles	[150]
SnSb/C	[15 wt% PAN (100% SnO2/Sb2O5)]/DMF	Not Specified	Stabilized at 250 °C for 2.5 hrs and carbonized at 700 °C for 2 hrs	345 mAh g^1 after 50 cycles	[150]
SnSb/C	[15 wt% PAN (100% SnO2/Sb2O5)]/DMF (Carbon Coated)	Not Specified	Stabilized at 250 °C for 2.5 hrs and carbonized at 700 °C for 2 hrs	781 mAh g^1 after 50 cycles	[150]
SnSb/rGO	[13 wt% PAN (1:1: 2 wt ratio Sn(CH3COO)/Sb (CH3COO)3/PAN)]/DMF (Carbon Coated)	4000 rpm	Stabilized at 280 °C for 2.5 hrs and carbonized at 700 °C for 1 hrs	324.5 mAh g^{-1} after 200 cycles	[151]

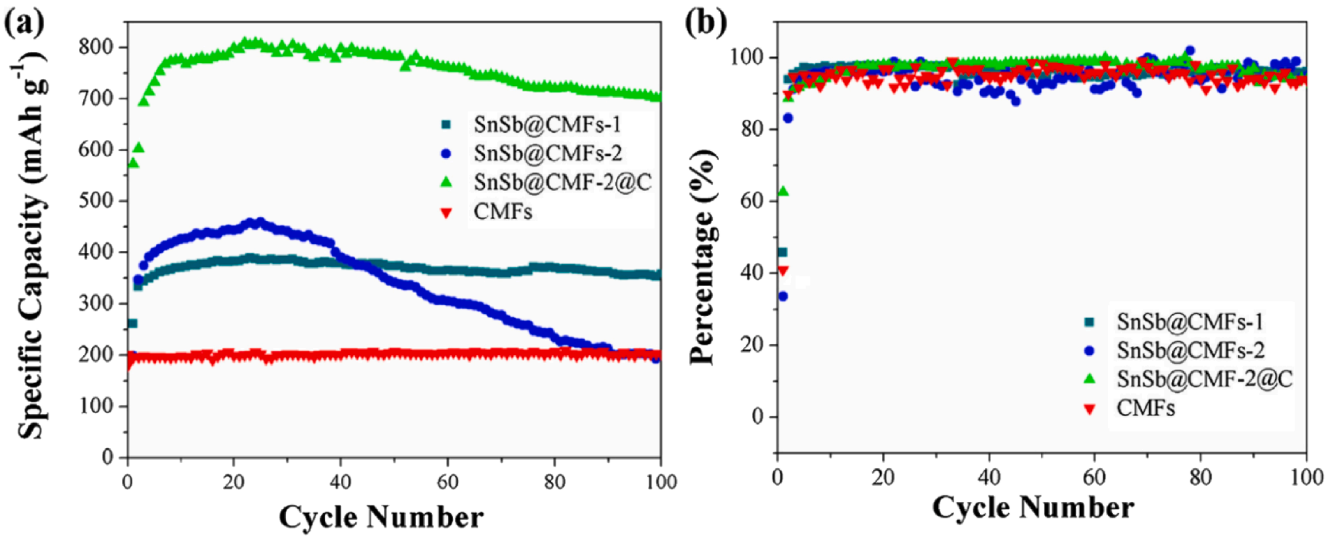

Fig. 16. a) Cycle performance and b) coulombic efficiencies plots for centrifugally spun SnSb@CMF-1, SnSb@CMF-2, SnSb@CMF-2@C composite-fibers, and carbon-fiber anodes. After Jia et al. [150] with permission.

dispersion of SnSb nanoparticles and constant capacity (~200 mAh g^{-1}) was observed in the SnSb@CMF-1, its capacity was ultimately lower than the SnSb@CMF-2@C composite-fiber anodes due to the lower active material loading in the carbon-fiber matrix. On the other hand, the higher active material loading in the SnSb@CMF-2 composite-fiber anode exposed more active material to the lithiation process, but it also formed agglomerations of SbSn nanoparticles in the carbon fiber matrix that led to higher capacities accompanied by volume changes that eventually lead to the collapse of the electrode. Hence, the carbon coating on the SnSb@CMF-2 helped confine the SnSb nanoparticles on the surface of the fibers as a conductive matrix which allowed a volume expansion during cycling [150].

In a similar study, SnSb@reduced graphene oxide@carbon microfibers (SnSb@rGO@CMF) were centrifugally spun. The addition of rGO is expected to improve the performance of these SIB anodes due to their superior chemical stability, electrical conductivity, and high specific area [151]. Similar conditions were used while preparing the SnSb@rGO@CMF and SnSb@CMFs with the rGO as the only variant. After 200 cycles at a galvanostatic 50 mAh g^{-1} current density, the SnS@CMFs showed a capacity of 289.8 mAh g^{-1} while the Sn/rGO/CMFs showed a capacity of 324.5 mAh g^{-1} [151]. The electrochemical results of these batteries are shown in Fig. 17a and b. The introduction of reduced graphene oxide helped attain a larger reversible capacity after 200 cycles due to the increased conductivity of the anodes, which improved the transport of Na^+.

3.3.2. *Carbon/metal-oxide composites*

Only two metal oxide materials have been used in the preparation of composite-fiber anodes via CS for SIBs. Also, multiple material compositions, additives, or further treatments were involved. A concise list of this material configuration and their electrochemical performance results are collected in Table 5.

3.3.2.1. SnO_2/C. SnO_2 is a metal oxide based on the alloying/dealloying reaction mechanism. Thus, in the reactions taking place on the electrode, Na_2O is formed as an inactive byproduct followed by the alloying/dealloying process between Na and Sn. The irreversible conversion reactions that form Na_2O take place during the first cycle (formation cycle) and can deliver a theoretical capacity of 710 mAh g^{-1} (Eq. (6) and (7)) [155]. Once these byproducts have formed, the reversible alloying reaction shown in Eq. (8) takes place.

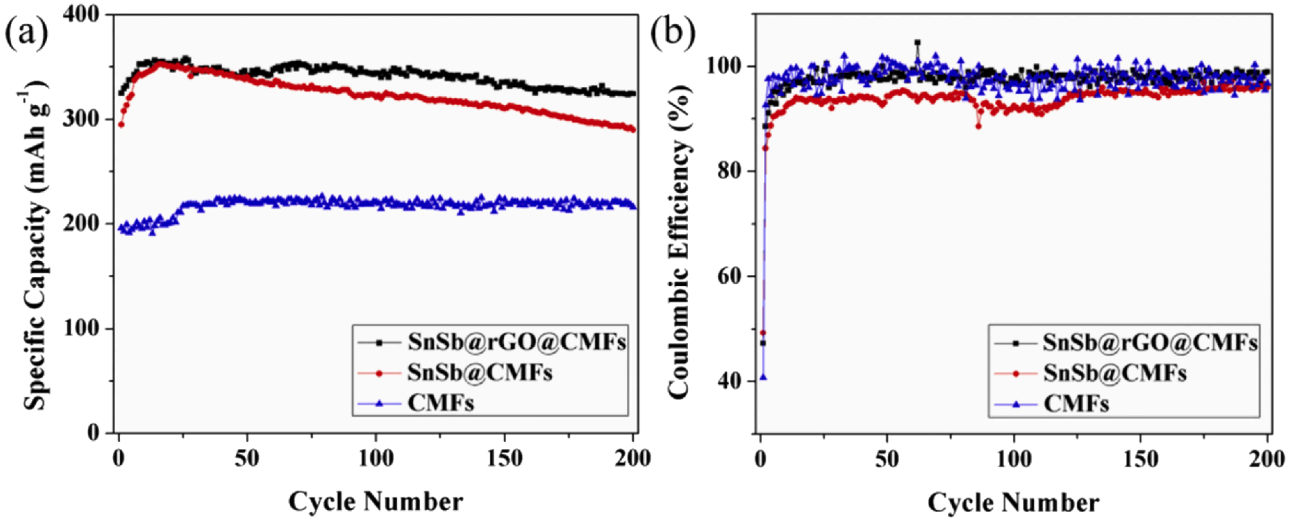

Fig. 17. a) Cycle performance and b) coulombic efficiency for CMFs, SnSb/CMFs, and SnSb/rGO/CMFs. After Jia et al. [151] with permission.

Table 5
Transition metal oxides used in the preparation of composite fibers via centrifugal spinning for use as anodes in SIBs.

Composite fiber anode material	Polymer Precursor(s), Additive(s), and Solvent(s)	Spinning Conditions	Stabilization and Carbonization	Electrochemical Performance	Reference
SnO_2/C	[12 wt% PAN (15 wt% SnO_2)]/DMF	7,000 rpm	Stabilized at 280 °C for 5 hrs and carbonized at 700 °C for 2 hrs	198 mAh g^1 after 50 cycles (Tested at 100 mA g^1)	[119]
SnO_2/C	Not Specified	Not Specified	Oxidized at 500 °C for 3 hrs	158 mAh g^1 after 50 cycles (tested at 640 mA g^1)	[153]
SnO_2/C & SnO_2/C CVD treated	[13 wt% PAN (40 wt% $SnCl_2$)]/DMF	4000 rpm	Oxidized at 500 °C for 3 hrs CVD for 30 60 and 90 mins.	71, 111, 158, 147 mAh g^{-1} after 30 cycles (tested at 40 mA g^{-1})	[154]
SnO_2/C & SnO_2/C CVD treated	[13 wt% PAN (40 wt% $SnCl_2$)]/DMF	4000 rpm	Oxidized at 500 °C for 3 hrs CVD for 30 60 and 90 mins.	39, 99, 86, 100 mAh g^{-1} after 50 cycles (tested at 640 mAh g^1)	[154]
MoO_2/C	[12 wt% PAN (80 wt%. MoO2)]/DMF	6,800 rpm	Stabilized at 280 °C for 5 hrs and carbonized at 700 °C for 2 hrs	~130 mAh g^{-1} after 100 cycles (tested at 100 mA g^1)	[120]

$$SnO_2 + 2Na^+ + 2e^- \rightarrow SnO + Na_2O \quad (6)$$

$$SnO + 2Na^+ + 2e^- \rightarrow Sn + Na_2O \quad (7)$$

$$Sn + xNa^+ + xe^- \leftrightarrow Na_xSn(0 \leq x \leq 3.75) \quad (8)$$

Thus, Sn can accommodate up to $3.75Na^+$ which in turn leads to a large volume expansion (<400%) [155]. Nonetheless, the large abundance, long cycle life, and high theoretical capacity during the alloying/dealloying process of Sn (667 mAh g^{-1}) are some of the reasons why SnO_2 has gained much interest for SIB applications [119,105,155]. Several research efforts have focused on employing CS to prepare composite SnO_2/C composite fibers as anode materials for SIB. SnO_2/C composite-fiber anodes were prepared by CS and subsequent heat treatment for use as anodes in Na-ion half cells. The SnO_2/C composite anode delivered a specific capacity of 198 mAh g^{-1} after 50 cycles at a current density of 100 mA g^{-1} over a voltage window between 0.05 and 2.5 V [119]. After the formation of the SEI layer during the first cycle, the cycle performance remained constant for the following 50 cycles. In a different study, SnO_2/C composite fibers were also prepared by CS and subsequent thermal treatment. The SnO_2/C composite-fiber anodes were tested at a constant current density and their performance was compared to that of the SnO_2 electrode. The results in Fig. 18 show that after 30 cycles at a current density of 20 mAg^{-1}, the specific discharge capacity of SnO_2/C composite-fiber anode and SnO_2 electrode were 216 mAh g^{-1} and 158 mAh g^{-1}, respectively [153]. Similarly, Fig. 19 shows that after 50 cycles at a current density of $640mAg^{-1}$, the specific discharge capacity of SnO_2/C composite fibers and SnO_2 electrodes were 158 mAh g^{-1} and 36 mAh g^{-1}, respectively [153].

In a further study, the authors investigated the electrochemical performance of centrifugally spun SnO_2/C composite anodes with and without a carbon vapor deposition (CVD) treatment [154]. Four anodes were prepared, which consisted of non-CVD treated SnO_2/C composite microfibers, and CVD-treated SnO_2/C composite microfibers for 30, 60, and 90 min [154]. Fig. 20 shows the specific discharge capacities for all four composite anodes after 30 cycles at a 40 mA g^{-1} current density which delivered 71, 111, 158, and 147 mAh g^{-1}, respectively [154]. Moreover, the SnO_2 composite fibers, treated with CVD and non-treated, were also tested at 640 mA g^{-1} and delivered specific discharge capacities of 39, 99, 86, and 100 mAh g^{-1} after 60 cycles, respectively [154]. Fig. 21 shows the cycle performance of all four anodes at a current density of 640 mA g^{-1}. A common pattern observed at both current rates is that the 90 min CVD treated fibers suffered the least capacity fading. On the other hand, the non-CVD treated anodes delivered the lowest discharge capacities using both current densities. At 40 mA g^{-1}, the non-CVD treated anodes showed an incremental specific discharge capacity, but they suffered from a sharp loss in capacity at around the 10th cycle. This can be attributed to the large volume change of Sn, which led to the pulverization of the anode and crumbling of the active material. At 640 mA g^{-1}, the non-CVD treated anodes did not show an increase or loss in capacity. This could be attributed to the fast rate of lithiation which overwhelmed the anode's ability to alloy with Na ions. On the other hand, the CVD-treated composite fibers were capable to perform better at higher current rates due to the increased conductivity and structural support of the CVD layer.

3.3.2.2. MoO_2/C. MoO_2, like many other materials, suffers from a substantial volume change during charge/discharge cycles. However, MoO_2 has gained attention as an anode material for SIBs because it is among some of the pseudocapacitive materials which can successfully improve the rate capability of SIBs [156]. Centrifugally spun MoO_2/C composite fibers were prepared and used as anode materials in Na-ion half-cells. The charge/discharge profiles and cycling performance results are shown in Fig. 22a and b, respectively. The MoO_2/C composite-fiber anode delivered a capacity of ~130 mAh g^{-1} after 100 cycles at 100 m Ag^1. A capacity recovery after the second cycle was observed [120]. This stability in capacity after the second cycle could be

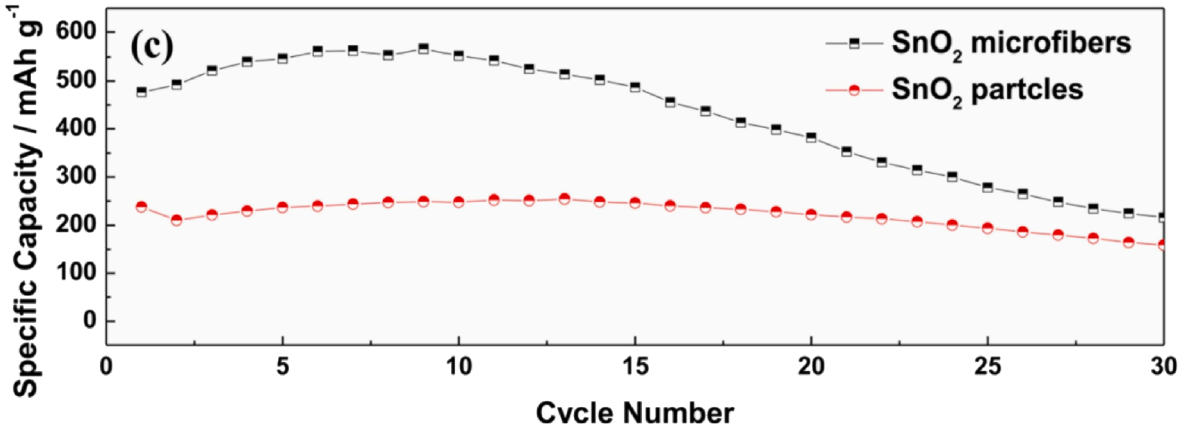

Fig. 18. Cycle performance for SnO_2/C composite-fiber anodes and SnO_2 electrodes at a 20 mAg^{-1} current density. After Lu et al. [153] with permission.

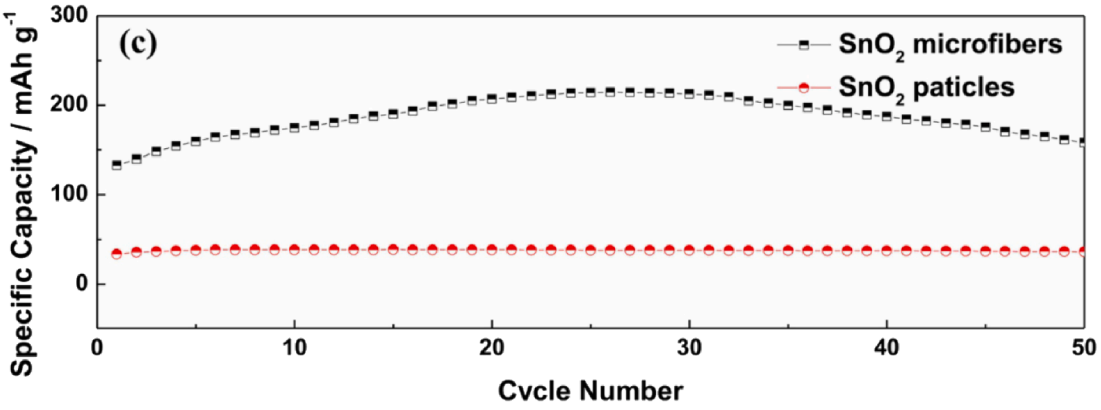

Fig. 19. Cycle performance for SnO_2/C composite-fiber anodes and SnO_2 electrodes at a 640 mAg^{-1} current density. After Lu et al. [153] with permission.

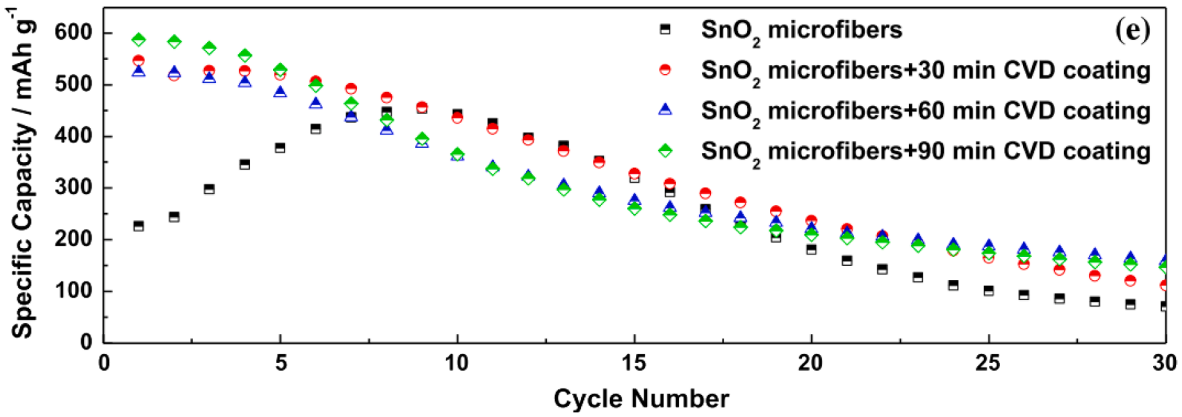

Fig. 20. Cycle performance for non-CVD, 30, 60, and 90 mins CVD-treated SnO_2/C composite anodes.at a 40 mAg^{-1} current density. After Lu et al. [154] with permission.

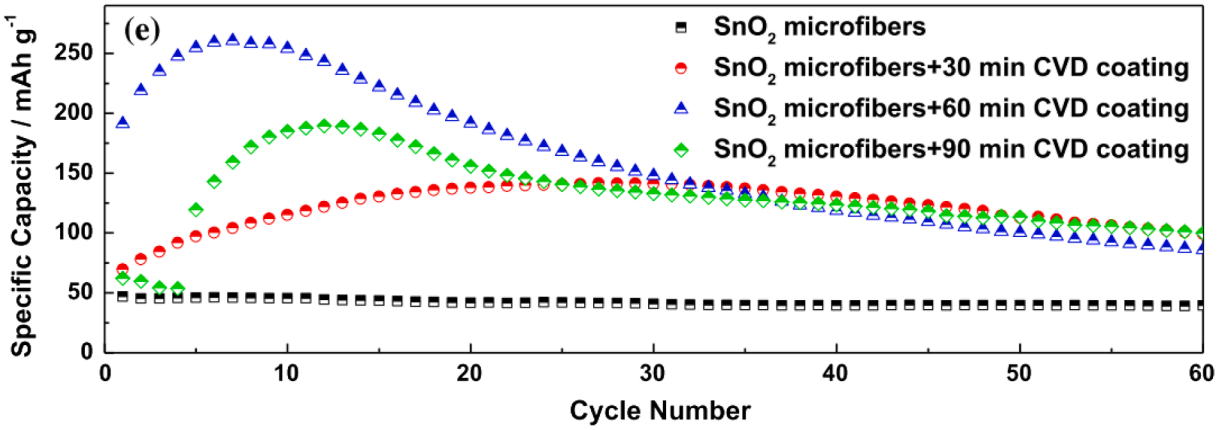

Fig. 21. Cycle performance for non-CVD, 30, 60, and 90 mins CVD-treated SnO_2/C composite anodes.at a 640 mAg^{-1} current density. After Lu et al. with permission [154] with permission.

attributed to the fast stabilization of the volume expansions and the improved conductivity of the composite fibers by the addition of MoO_2.

3.3.3. *Discussions on composite carbon fibers for SIBs*

Compared to LIB anodes, there is more room for innovation in SIBs since not as many materials or fiber structures have been investigated. In this text, only three materials were discussed, SnO_2, MoO_2, and SnSb. The centrifugally spun SnO_2/C composite anodes delivered a specific capacity of 198 mAh g^{-1} after 50 cycles at 100 mAg^{-1} [119]. Besides centrifugally spun fibers, electrospun SnO_2/C composite-fiber anodes have exhibited higher capacities in part due to the nature of the processing method. For example, partially reduced SnO_2 nanoparticles were embedded in carbon fibers followed by carbon coating and thermal reduction processes [157]. After 50 cycles at a current density of 100 mA g^{-1}, the SnO_2/C composite-fiber electrode delivered a high specific capacity of 536 mAh g^{-1} at 100 mA g^{-1} [157]. This comparison illustrates how further fiber treatments could improve the performance of not only the electrospun fibers but also the centrifugally spun fibers as

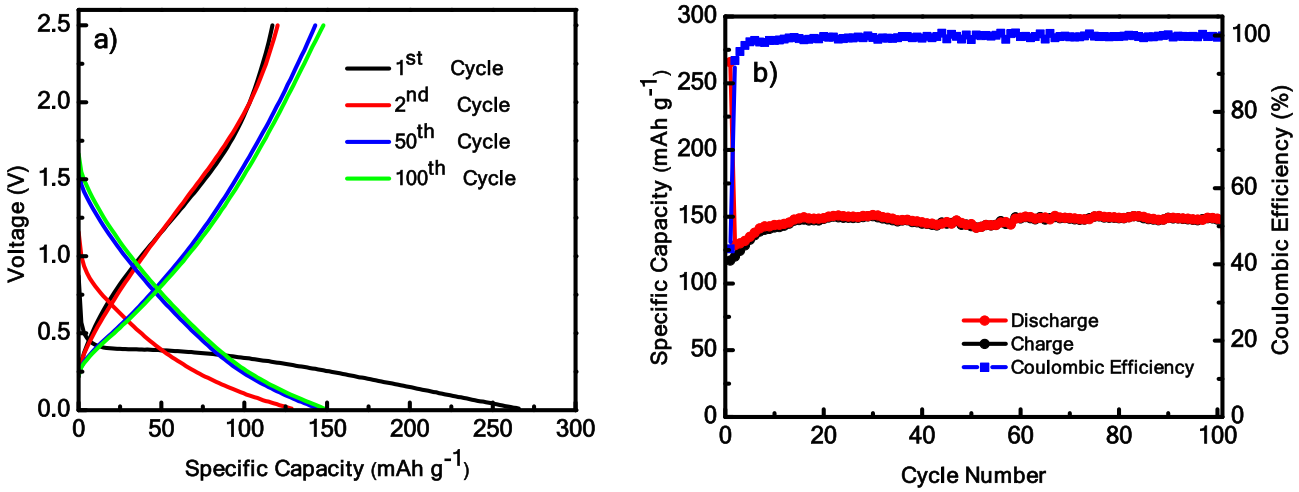

Fig. 22. a) Charge/discharge and b) cycle performance of MoO_2/C composite anode in half-cell SIBs. After Valdez et al. [120] with permission.

well. Another comparison is the use of sulfur-doped MoO_2/C composite electrospun fibers as anodes for SIBs. The sulfur doping process can improve the electronic conductivity of the carbon matrix, which in turn increases the intercalation of active material with Na^+ [158]. Lastly, as mentioned in the previous section, centrifugally spun SnSb/C composite-fiber anodes yielded a capacity of 345 mAh g^{-1} after 50 cycles at a current density of 100 mA g^{-1} [150]. Similar experiments have been conducted by the electrospinning and subsequent thermal treatment. In this study, $SnCl_2$ and $SbCl_3$ were used as precursors of the SnSb alloy. Also, TEOS was included in the solution as the silica precursor. All these precursors were homogenized in a PVP/DMF solution from which electrospun porous SnSb/SiO2/C CFs were obtained [159]. The incorporation of silica in the carbon matrix helped to buffer the volume change and maintained the structural integrity of the fibers [159]. The SnSb/SiO_2/C composite fiber anode exhibited a high specific capacity of 660 mAh g^{-1} at a galvanostatic current density of 200 mA g^{-1} after 100 cycles [159]. As one can observe for the SnSb binder-free anodes, the addition of TEOS resulted in a significant improvement in the electrochemical performance of electrospun composite fibers. Nevertheless, the centrifugal spinning method offers a much higher production rate than electrospinning, which could enable these material improvement steps to be adopted by the industry for the large production rate of composite fibers for LIBs and SIBs.

It is worthwhile to mention here that most of electrochemical performance experiments reported in this work (Tables 1 to 5) on centrifugally spun composite-fiber anodes for LIBs and SIBs were performed at $\leq$ 100 cycles. It is common in electrochemical research to show the cycle performance of Li-ion and Na-ion half cells for 100 cycles, so that the effect of the SEI formation and volume change can be observed during the first few cycles. The active material in composite-fiber anodes that provoke a large volume expansion/contraction during cycling can lead to a sudden irreversible capacity and capacity fading due to pulverization of the fiber structure or crumbling of the SEI layer. Such cases would be found in anodes with an alloying reaction mechanism (i.e., Si, Sn, SnO_2, Sb) and/or some metal oxides. Thus, for these cases, the capacity before anode collapse or capacity fading due to the large volume change is usually observed in the first 1–100 cycles (presumably between 50 and 100 cycles) and sometimes in the first few cycles. For example, low capacity anode materials such as graphite (with a theoretical capacity of 370 mAg^{-1}) can show a stable capacity after 10 cycles, therefore there is no need to show the capacity of carbon-based anodes for at higher cycle numbers > 50 cycles since the volume change is small compared to, for example, Si or Sn-based anodes. For active materials with a high-volume change, there will always be a loss in capacity during the first few cycles caused by the SEI formation and volume change. In some cases, such as for the results shown in Fig. 13, the anode shows an increased capacity with increasing cycle number, which is due to the fact that the active material gets more access to the electrolyte upon cycling. This phenomenon can be considered as an activation process due to the aggregation of the nanoparticles/particles (active material) in the fiber matrix and after a few cycles, the aggregated nanoparticles pulverize into smaller clusters as a result of the volume change of the anode, leading to the exposure of more active material (nanoparticles/particles) to the electrolyte, thus resulting in increased capacity [160–162,121]. In this case, it is important to show the cycling stability of the anode at higher cycle numbers as it is observed in Fig. 13 where the authors show the cycle performance of the composite-fiber anodes up to 400 cycles where the anode shows a stable capacity after about 300 cycles [121]. For example, if the anode shows a cycle stability after 50 cycles, this means that there is no need to do the experiments at (>100 cycles). Keeping in mind that performing the charge/discharge experiments at high cycle numbers is time consuming especially at slow charge/discharge rates.

4. Conclusions

The centrifugal spinning and subsequent heat treatment of polymer composite precursors can result in composite fibers-with improved electrochemical performance for use as anode materials in LIBs and SIBs. The improved performance of centrifugally spun composite fibers is attributed to the high surface-to-volume ratio of the fibers and the elimination of the use of binders or conductive additives during the preparation of the electrode. Compared to electrospinning, centrifugal spinning can produce tens of grams of micro/nanofibers per hour. Thus, this method could potentially fulfill the production rate demand at an industrial scale. Based on the advantages of the centrifugal spinning over electrospinning, it was concluded that with centrifugal spinning systems, a higher fiber yield rate, safer, and less expensive production process can be achieved. Hence, a shift in popularity from electrospinning to centrifugal spinning could be seen in the future. Furthermore, hybrid versions that combine centrifugal spinning and electrospinning are emerging [163]. The main objective of this hybrid system is to increase fiber production through centrifugal spinning while improving the distribution and orientation of conductive fillers. Namely, this new approach is called centrifugal electrospinning and it is in its rudimentary stages [163]. However, with the current centrifugal spinning capabilities, fibers with different morphology and structures, including but not limited to carbon fibers and composite carbon fibers, have been recently used as electrode materials for LIBs and SIBs. Based on the results and discussions on the production of composite fibers for LIBs and SIBs presented in this work, it can be concluded that centrifugal

spinning opens a new approach to manufacture anodes at a large industrial scale and a wide window of opportunity for innovation still open for those looking to implement this technology in future applications.

Declaration of Competing Interest

The authors declare that they have no known competing financial interests or personal relationships that could have appeared to influence the work reported in this paper.

Acknowledgments

This research was supported by National Science Foundation (NSF) PREM award under grant No. DMR-1523577: UTRGV-UMN Partnership for Fostering Innovation by Bridging Excellence in Research and Student Success. Part of this work was carried out in the College of Science and Engineering Characterization Facility, University of Minnesota, which has received capital equipment funding from the NSF through the UMN MRSEC program under Award Number DMR-2011401.

References

[1] P. Arora, Z.M. Zhang, Battery separators, Chem. Rev. 104 (2004) 4419–4462.
[2] C.F. Liu, Z.G. Neale, G.Z. Cao, Understanding electrochemical potentials of cathode materials in rechargeable batteries, Mater. Today 19 (2016) 109–123.
[3] S. Sharma, A.K. Panwar, M.M. Tripathi, Storage technologies for electric vehicles, J. Traffic Transp. Eng. 7 (2020) 340–361.
[4] P.Z. Lyu, X.J. Liu, J. Qu, J.T. Zhao, Y.T. Huo, Z.G. Qu, Z.H. Rao, Recent advances of thermal safety of lithium ion battery for energy storage, Energy Storage Mater. 31 (2020) 195–220.
[5] M.D. Slater, D. Kim, E. Lee, C.S. Johnson, Sodium-ion batteries, Adv. Funct. Mater. 23 (2013) 947–958.
[6] C. Yang, S. Xin, L.Q. Mai, Y. You, Materials Design for High-Safety Sodium-Ion Battery, Adv Energy Mater, DOI ARTN 2000974 10.1002/aenm.202000974 (2020).
[7] M.A. Munoz-Marquez, D. Saurel, J.L. Gomez-Camer, M. Casas-Cabanas, E. Castillo-Martinez, T. Rojo, Na-ion batteries for large scale applications: a review on anode materials and solid electrolyte interphase formation, Adv. Energy Mater. 7 (2017).
[8] N. Yabuuchi, K. Kubota, M. Dahbi, S. Komaba, Research development on sodium-ion batteries, Chem. Rev. 114 (2014) 11636–11682.
[9] X.M. Yang, A.L. Rogach, Anodes and sodium-free cathodes in sodium ion batteries, Adv. Energy Mater. 10 (2020).
[10] B.W. Xiao, T. Rojo, X.L. Li, Hard carbon as sodium-ion battery anodes: progress and challenges, ChemSusChem 12 (2019) 133–144.
[11] Y.Q. Li, L. Yu, W.R. Hu, X.L. Hu, Thermotolerant separators for safe lithium-ion batteries under extreme conditions, J. Mater. Chem. A 8 (2020) 20294–20317.
[12] V.A. Agubra, D. De la Garza, L. Gallegos, M. Alcoutlabi, ForceSpinning of polyacrylonitrile for mass production of lithium-ion battery separators, J. Appl. Polym. Sci. 133 (2016).
[13] X.W. Zhang, L.W. Ji, O. Toprakci, Y.Z. Liang, M. Alcoutlabi, Electrospun nanofiber-based anodes cathodes, and separators for advanced lithium-ion batteries, Polym. Rev. 51 (2011) 239–264.
[14] L.W. Ji, P. Meduri, V. Agubra, X.C. Xiao, M. Alcoutlabi, Graphene-based nanocomposites for energy storage, Adv. Energy Mater. 6 (2016).
[15] J.H. Chen, A. Naveed, Y. Nuli, J. Yang, J.L. Wang, Designing an intrinsically safe organic electrolyte for rechargeable batteries, Energy Storage Mater. 31 (2020) 382–400.
[16] J.J. Zhang, L.P. Yue, Q.S. Kong, Z.H. Liu, X.H. Zhou, C.J. Zhang, Q. Xu, B. Zhang, G.L. Ding, B.S. Qin, Y.L. Duan, Q.F. Wang, J.H. Yao, G.L. Cui, L.Q. Chen, Sustainable, heat-resistant and flame-retardant cellulose-based composite separator for high-performance lithium ion battery, Sci. Rep.-UK 4 (2014).
[17] M. Yanilmaz, Y. Lu, Y. Li, X.W. Zhang, SiO2/polyacrylonitrile membranes via centrifugal spinning as a separator for Li-ion batteries, J. Power Sour. 273 (2015) 1114–1119.
[18] M.T. McDowell, S.W. Lee, W.D. Nix, Y. Cui, 25th anniversary article: understanding the lithiation of silicon and other alloying anodes for lithium-ion batteries, Adv. Mater. 25 (2013) 4966–4984.
[19] Y.L. Wang, B.X. Liu, G.F. Tian, S.L. Qi, D.Z. Wu, Research progress of cathode binder for high performance lithium-ion battery, Acta Polym. Sin. 51 (2020) 326–337.
[20] J.T. Li, Z.Y. Wu, Y.Q. Lu, Y. Zhou, Q.S. Huang, L. Huang, S.G. Sun, Water soluble binder, an electrochemical performance booster for electrode materials with high energy density, Adv. Energy Mater. 7 (2017).
[21] Y. Lu, K. Fu, S. Zhang, Y. Li, C. Chen, J.D. Zhu, M. Yanilmaz, M. Dirican, X. W. Zhang, Centrifugal spinning: a novel approach to fabricate porous carbon fibers as binder-free electrodes for electric double-layer capacitors, J. Power Sour. 273 (2015) 502–510.
[22] M. Dirican, X.W. Zhang, Centrifugally-spun carbon microfibers and porous carbon microfibers as anode materials for sodium-ion batteries, J. Power Sour. 327 (2016) 333–339.
[23] T. Hou, X.L. Li, Y.S. Lu, B. Yang, Highly porous fibers prepared by centrifugal spinning, Mater Design 114 (2017) 303–311.
[24] L. Xia, J.G. Ju, W. Xu, C.K. Ding, B.W. Cheng, Preparation and characterization of hollow Fe2O3 ultra-fine fibers by centrifugal spinning, Mater Design 96 (2016) 439–445.
[25] R.G. Jorge Lopez, Jonathan Ayala, Jesus Cantu, Alexandria Castillo, Jason Parsons, Jason Myers, Timothy P.Lodge, Mataz Alcoutlabi, Centrifugally spun TiO2/C composite fibers prepared from TiS2/PAN precursor fibers as binder-free anodes for LIBS, Journal of Physics and Chemistry of Solids, 149 (2021) 109795.
[26] L.W. Ji, Z. Lin, M. Alcoutlabi, X.W. Zhang, Recent developments in nanostructured anode materials for rechargeable lithium-ion batteries, Energy Environ. Sci. 4 (2011) 2682–2699.
[27] B.S. Lee, A review of recent advancements in electrospun anode materials to improve rechargeable lithium battery performance, Polym. Basel 12 (2020).
[28] L. Lavagna, G. Meligrana, C. Gerbaldi, A. Tagliaferro, M. Bartoli, Graphene and lithium-based battery electrodes: a review of recent literature, Energies 13 (2020).
[29] E. Peled, D. Golodnitsky, G. Ardel, Advanced model for solid electrolyte interphase electrodes in liquid and polymer electrolytes, J. Electrochem. Soc. 144 (1997) L208–L210.
[30] H.C. Yang, J. Li, Z.H. Sun, R.P. Fang, D.W. Wang, K. He, H.M. Cheng, F. Li, Reliable liquid electrolytes for lithium metal batteries, Energy Storage Mater. 30 (2020) 113–129.
[31] J.B. Goodenough, Electrochemical energy storage in a sustainable modern society, Energy Environ. Sci. 7 (2014) 14–18.
[32] X.W. Zhang, Y. Lu, Centrifugal spinning: an alternative approach to fabricate nanofibers at high speed and low cost, Polym. Rev. 54 (2014) 677–701.
[33] X.J. Wang, Y.C. Liu, Y.J. Wang, L.F. Jiao, CuO quantum dots embedded in carbon nanofibers as binder-free anode for sodium ion batteries with enhanced properties, Small 12 (2016) 4865–4872.
[34] S.H. Chen, L. Qiu, H.M. Cheng, Carbon-based fibers for advanced electrochemical energy storage devices, Chem. Rev. 120 (2020) 2811–2878.
[35] D.A. Notter, M. Gauch, R. Widmer, P. Wager, A. Stamp, R. Zah, H.J. Althaus, Contribution of li-ion batteries to the environmental impact of electric vehicles, Environ. Sci. Technol. 44 (2010) 6550–6556.
[36] N.E. Zander, Formation of melt and solution spun polycaprolactone fibers by centrifugal spinning, J. Appl. Polym. Sci. 132 (2015).
[37] J.M. Jiang, G.D. Nie, P. Nie, Z.W. Li, Z.H. Pan, Z.K. Kou, H. Dou, X.G. Zhang, J. Wang, Nanohollow carbon for rechargeable batteries: ongoing progresses and challenges, Nano-Micro Lett. 12 (2020).
[38] T.H. Cho, M. Tanaka, H. Onishi, Y. Kondo, T. Nakamura, H. Yamazaki, S. Tanase, T. Sakai, Battery performances and thermal stability of polyacrylonitrile nanofiber-based nonwoven separators for Li-ion battery, J. Power Sour. 181 (2008) 155–160.
[39] T. Dong, W. Ul Arifeen, J. Choi, K. Yoo, T. Ko, Surface-modified electrospun polyacrylonitrile nano-membrane for a lithium-ion battery separator based on phase separation mechanism, Chem. Eng. J. 398 (2020).
[40] S.S. Zhang, A review on the separators of liquid electrolyte Li-ion batteries, J. Power Sour. 164 (2007) 351–364.
[41] A.A. Heidari, H. Mahdavi, Recent development of polyolefin-based microporous separators for li-ion batteries: a review, Chem. Rec. 20 (2020) 570–595.
[42] R.H. Lv, Y. Zhu, H.S. Liu, B. Na, Y.H. Huang, X.L. Xie, Poly(vinylidene fluoride)/poly(acrylonitrile) blend fibrous membranes by centrifugal spinning for high-performance lithium ion battery separators, J. Appl. Polym. Sci. 134 (2017).
[43] H. Lee, M. Yanilmaz, O. Toprakci, K. Fu, X.W. Zhang, A review of recent developments in membrane separators for rechargeable lithium-ion batteries, Energy Environ. Sci. 7 (2014) 3857–3886.
[44] X.H. Rui, H.T. Tan, Q.Y. Yan, Nanostructured metal sulfides for energy storage, Nanoscale 6 (2014) 9889–9924.
[45] P. Poizot, S. Laruelle, S. Grugeon, L. Dupont, J.M. Tarascon, Nano-sized transition-metaloxides as negative-electrode materials for lithium-ion batteries, Nature 407 (2000) 496–499.
[46] X.Z. Li, M. Zhang, S.X. Yuan, C.X. Lu, Research progress of silicon/carbon anode materials for lithium-ion batteries: structure design and synthesis method, Chemelectrochem 7 (2020) 4289–4302.
[47] M.A. Kebede, Tin oxide-based anodes for both lithium-ion and sodium-ion batteries, Curr. Opin. Electrochem. 21 (2020) 182–187.
[48] D. Larcher, S. Beattie, M. Morcrette, K. Edstroem, J.C. Jumas, J.M. Tarascon, Recent findings and prospects in the field of pure metals as negative electrodes for Li-ion batteries, J. Mater. Chem. 17 (2007) 3759–3772.
[49] L. Fei, B.P. Williams, S.H. Yoo, J. Kim, G. Shoorideh, Y.L. Joo, Graphene folding in Si rich carbon nanofibers for highly stable, high capacity li-ion battery anodes, Acs Appl. Mater. Inter. 8 (2016) 5243–5250.
[50] X.H. Huang, J.P. Tu, B. Zhang, C.Q. Zhang, Y. Li, Y.F. Yuan, H.M. Wu, Electrochemical properties of NiO-Ni nanocomposite as anode material for lithium ion batteries, J. Power Sour. 161 (2006) 541–544.
[51] X. Xu, W. Liu, Y. Kim, J. Cho, Nanostructured transition metal sulfides for lithium ion batteries: Progress and challenges, Nano Today 9 (2014) 604–630.
[52] X.B. Hao, Y.C. Zeng, A review on the studies of air flow field and fiber formation process during melt blowing, Ind. Eng. Chem. Res. 58 (2019) 11624–11637.
[53] V.A. Wente, Superfine thermoplastic fibers, Ind. Eng. Chem. 48 (1956) 1342–1346.

[54] E. Stojanovska, E. Canbay, E.S. Pampal, M.D. Calisir, O. Agma, Y. Polat, R. Simsek, N.A.S. Gundogdu, Y. Akgul, A. Kilic, A review on non-electro nanofibre spinning techniques, RSC Adv. 6 (2016) 83783–83801.

[55] X.S. Huang, Separator technologies for lithium-ion batteries, J. Solid State Electr 15 (2011) 649–662.

[56] Y. Kawahara, W. Takarada, K. Takeda, Y. Ikeda, K. Onda, T. Kikutani, Dyeing Behavior and Multi-Functionalities of Polylactide/Poly (Ethylene Terephthalate) Conjugate Fibers Produced by High-Speed Melt-Spinning, J Macromol Sci B, DOI 10.1080/00222348.2020.1819665(2020).

[57] J.N. Song, Z.W. Li, H. Wu, Blowspinning: a new choice for nanofibers, Acs Appl. Mater. Inter. 12 (2020) 33447–33464.

[58] T. Kikutani, J. Radhakrishnan, S. Arikawa, A. Takaku, N. Okui, X. Jin, F. Niwa, Y. Kudo, High-speed melt spinning of bicomponent fibers: Mechanism of fiber structure development in poly(ethylene terephthalate)/polypropylene system, J. Appl. Polym. Sci. 62 (1996) 1913–1924.

[59] M. Naeimirad, A. Zadhoush, R. Kotek, R.E. Neisiany, S.N. Khorasani, S. Ramakrishna, Recent advances in core/shell bicomponent fibers and nanofibers: a review, J. Appl. Polym. Sci. 135 (2018).

[60] M.A. Hunt, T. Saito, R.H. Brown, A.S. Kumbhar, A.K. Naskar, Patterned functional carbon fibers from polyethylene, Adv. Mater. 24 (2012) 2386–2389.

[61] J. Sheng, S.H. Tong, Z.B. He, R.D. Yang, Recent developments of cellulose materials for lithium-ion battery separators, Cellulose 24 (2017) 4103–4122.

[62] J.H. Zhao, W.Q. Han, H.D. Chen, M. Tu, R. Zeng, Y.F. Shi, Z.G. Cha, C.R. Zhou, Preparation, structure and crystallinity of chitosan nano-fibers by a solid-liquid phase separation technique, Carbohyd Polym 83 (2011) 1541–1546.

[63] L.M. He, Y.Q. Zhang, X. Zeng, D.P. Quan, S. Liao, Y.S. Zeng, J. Lu, S. Ramakrishna, Fabrication and characterization of poly(L-lactic acid) 3D nanofibrous scaffolds with controlled architecture by liquid-liquid phase separation from a ternary polymer-solvent system, Polymer 50 (2009) 4128–4138.

[64] J.T. Jung, J.F. Kim, H.H. Wang, E. di Nicolo, E. Drioli, Y.M. Lee, Understanding the non-solvent induced phase separation NIPS) effect during the fabrication of microporous PVDF membranes via thermally induced phase separation (TIPS), J. Membr. Sci. 514 (2016) 250–263.

[65] Q.Y. Wu, H.Q. Liang, L. Gu, Y. Yu, Y.Q. Huang, Z.K. Xu, PVDF/PAN blend separators via thermally induced phase separation for lithium ion batteries, Polymer 107 (2016) 54–60.

[66] H.S. Jeong, D.W. Kim, Y.U. Jeong, S.Y. Lee, Effect of phase inversion on microporous structure development of Al2O3/poly(vinylidene fluoride-hexafluoropropylene)-based ceramic composite separators for lithium-ion batteries, J. Power Sour. 195 (2010) 6116–6121.

[67] L.P. Liu, Z. Wang, Z.K. Zhao, Y.J. Zhao, F. Li, L.B. Yang, PVDF/PAN/SiO2 polymer electrolyte membrane prepared by combination of phase inversion and chemical reaction method for lithium ion batteries, J. Solid State Electron. 20 (2016) 699–712.

[68] V. Kleivaite, R. Milasius, Electrospinning-100 years of investigations and still open questions of web structure estimination, Autex Res. J. 18 (2018) 398–404.

[69] W.E. Teo, S. Ramakrishna, A review on electrospinning design and nanofibre assemblies, Nanotechnology 17 (2006) R89–R106.

[70] H.M. Ibrahim, A. Klingner, A review on electrospun polymeric nanofibers: Production parameters and potential applications, Polym. Test. 90 (2020).

[71] C.J. Luo, S.D. Stoyanov, E. Stride, E. Pelan, M. Edirisinghe, Electrospinning versus fibre production methods: from specifics to technological convergence, Chem. Soc. Rev. 41 (2012) 4708–4735.

[72] J.W. Jung, C.L. Lee, S. Yu, I.D. Kim, Electrospun nanofibers as a platform for advanced secondary batteries: a comprehensive review, J. Mater. Chem. A 4 (2016) 703–750.

[73] H. Jiang, Y.Q. Ge, K. Fu, Y. Lu, C. Chen, J.D. Zhu, M. Dirican, X.W. Zhang, Centrifugally-spun tin-containing carbon nanofibers as anode material for lithium-ion batteries, J. Mater. Sci. 50 (2015) 1094–1102.

[74] Z. Yang, H.D. Peng, W.Z. Wang, T.X. Liu, Crystallization behavior of Poly(epsilon-caprolactone)/layered double hydroxide nanocomposites, J. Appl. Polym. Sci. 116 (2010) 2658–2667.

[75] V.A. Agubra, L. Zuniga, D. De la Garza, L. Gallegos, M. Pokhrel, M. Alcoutlabi, Forcespinning: A new method for the mass production of Sn/C composite nanofiber anodes for lithium ion batteries, Solid State Ionics 286 (2016) 72–82.

[76] S. Padron, A. Fuentes, D. Caruntu, K. Lozano, Experimental study of nanofiber production through forcespinning, J. Appl. Phys. 113 (2013).

[77] H.Z. Xu, H.H. Chen, X.L. Li, C. Liu, B. Yang, A comparative study of jet formation in nozzle- and nozzle-less centrifugal spinning systems, J. Polym. Sci. Polym. Phys. 52 (2014) 1547–1559.

[78] X.G. Zhang, J.X. Qiao, H. Zhao, Z.H. Huang, Y.G. Liu, M.H. Fang, X.W. Wu, X. Min, Preparation and performance of novel polyvinylpyrrolidone/polyethylene glycol phase change materials composite fibers by centrifugal spinning, Chem. Phys. Lett. 691 (2018) 314–318.

[79] N.E. Zander, M. Gillan, D. Sweetser, Composite fibers from recycled plastics using melt centrifugal spinning, Materials 10 (2017).

[80] G. Chen, T.T. Shi, X.G. Zhang, F. Cheng, X.W. Wu, G.Q. Leng, Y.G. Liu, M.H. Fang, X. Min, Z.H. Huang, Polyacrylonitrile/polyethylene glycol phase-change material fibres prepared with hybrid polymer blends and nano-SiC fillers via centrifugal spinning, Polymer 186 (2020).

[81] Z.W. Habibollah Aminirastabi, HaoXue, Yuxi Yu, Guoli Ji, Vojislav V. Mitic, Rengang Guan, Evaluation of nano grain growth of TiO2 fibers fabricated via centrifugal jet spinning, Nano-Structures & Nano-Objects, 21 (2020) 100413.

[82] M.D. Calisir, A. Kilic, A comparative study on SiO2 nanofiber production via two novel non-electrospinning methods: centrifugal spinning vs solution blowing, Mater. Lett. 258 (2020).

[83] L. Xia, L.L. Lu, Y.X. Liang, Preparation and characterization of poly(lactic acid) micro- and nanofibers fabricated by centrifugal spinning, Fiber Polym. 21 (2020) 1422–1429.

[84] H.M. Golecki, H.Y. Yuan, C. Glavin, B. Potter, M.R. Badrossamay, J.A. Goss, M. D. Phillips, K.K. Parker, Effect of solvent evaporation on fiber morphology in rotary jet spinning, Langmuir 30 (2014) 13369–13374.

[85] J.J. Rogalski, L. Botto, C.W.M. Bastiaansen, T. Peijs, A study of rheological limitations in rotary jet spinning of polymer nanofibers through modeling and experimentation, J. Appl. Polym. Sci. 137 (2020).

[86] X.L. Li, Y.S. Lu, T. Hou, J. Zhou, B. Yang, Centrifugally spun ultrafine starch/PEO fibres as release formulation for poorly water-soluble drugs, Micro Nano Lett. 13 (2018) 1688–1692.

[87] Z.M. Zhang, B.Y. Chen, Z.L. Lai, J.W. Wang, Y.S. Duan, Spinning solution flow model in the nozzle and experimental study of nanofibers fabrication via high speed centrifugal spinning, Polymer 205 (2020).

[88] S. Saha, P. Sadhukhan, S.R. Chowdhury, S. Das, Rotary-Jet spin assisted fabrication of MnO2 microfiber for supercapacitor electrode application, Mater. Lett. 277 (2020).

[89] M. Alcoutlabi, G.B. McKenna, Effects of confinement on material behaviour at the nanometre size scale, J. Phys.-Condens Mater. 17 (2005) R461–R524.

[90] Y.Z. Liang, L.W. Ji, B.K. Guo, Z. Lin, Y.F. Yao, Y. Li, M. Alcoutlabi, Y.P. Qiu, X. W. Zhang, Preparation and electrochemical characterization of ionic-conducting lithium lanthanum titanate oxide/polyacrylonitrile submicron composite fiber-based lithium-ion battery separators, J. Power Sour. 196 (2011) 436–441.

[91] S.V. Fridrikh, J.H. Yu, M.P. Brenner, G.C. Rutledge, Controlling the fiber diameter during electrospinning, Phys. Rev. Lett. 90 (2003).

[92] V. Poursorkhabi, M.A. Abdelwahab, M. Misra, H. Khalil, B. Gharabaghi, A. K. Mohanty, Processing, carbonization, and characterization of lignin based electrospun carbon fibers: a review, Front. Energy Res. 8 (2020).

[93] A. Koski, K. Yim, S. Shivkumar, Effect of molecular weight on fibrous PVA produced by electrospinning, Mater. Lett. 58 (2004) 493–497.

[94] A. Anceschi, F. Caldera, M. Bertasa, C. Cecone, F. Trotta, P. Bracco, M. Zanetti, M. Malandrino, P.E. Mallon, D. Scalarone, New poly(beta-cyclodextrin)/poly (vinyl alcohol) electrospun sub-micrometric fibers and their potential application for wastewater treatments, Nanomater. Basel 10 (2020).

[95] J.Y. Lin, B. Ding, J.Y. Yu, Y. Hsieh, Direct fabrication of highly nanoporous polystyrene fibers via electrospinning, ACS Appl. Mater. Inter. 2 (2010) 521–528.

[96] A. Mataz, The use of Fe3O4/Carbon composite fibers as anode materials in lithium ion batteries, MOJ Polym. Sci. 2 (2018).

[97] E.S. Pampal, E. Stojanovska, B. Simon, A. Kilic, A review of nanofibrous structures in lithium ion batteries, J. Power Sour. 300 (2015) 199–215.

[98] Y. Lu, Y. Li, S. Zhang, G.J. Xu, K. Fu, H. Lee, X.W. Zhang, Parameter study and characterization for polyacrylonitrile nanofibers fabricated via centrifugal spinning process, Eur. Polym. J. 49 (2013) 3834–3845.

[99] D. Flores, J. Villarreal, J. Lopez, M. Alcoutlabi, Production of carbon fibers through Forcespinning (R) for use as anode materials in sodium ion batteries, Mater. Sci. Eng. B-Adv. 236 (2018) 70–75.

[100] H.T. Niu, J. Zhang, Z.L. Xie, X.G. Wang, T. Lin, Preparation, structure and supercapacitance of bonded carbon nanofiber electrode materials, Carbon 49 (2011) 2380–2388.

[101] R.O.C.a.M. Alcoutlabi, Production of Carbon Fibers by Centrifugal Spinning of Aqueous PVP Solutions, in preparation (2020).

[102] L. Zuniga, V. Agubra, D. Flores, H. Campos, J. Villareal, M. Alcoutlabi, Multichannel hollow structure for improved electrochemical performance of TiO2/Carbon composite nanofibers as anodes for lithium ion batteries, J. Alloy. Compd. 686 (2016) 733–743.

[103] L.T. Dong, G.W. Wang, X.F. Li, D.B. Xiong, B. Yan, B.X. Chen, D.J. Li, Y.H. Cui, PVP-derived carbon nanofibers harvesting enhanced anode performance for lithium ion batteries, RSC Adv. 6 (2016) 4193–4199.

[104] C.K. Liu, Y. Feng, H.J. He, J. Zhang, R.J. Sun, M.Y. Chen, Effect of carbonization temperature on properties of aligned electrospun polyacrylonitrile carbon nanofibers, Mater Design 85 (2015) 483–486.

[105] J.C. Guo, A. Sun, C.S. Wang, A porous silicon-carbon anode with high overall capacity on carbon fiber current collector, Electrochem. Commun. 12 (2010) 981–984.

[106] X.S. Zhou, L.J. Wan, Y.G. Guo, Electrospun silicon nanoparticle/porous carbon hybrid nanofibers for lithium-ion batteries, Small 9 (2013) 2684–2688.

[107] M.S. Wang, W.L. Song, J. Wang, L.Z. Fan, Highly uniform silicon nanoparticle/porous carbon nanofiber hybrids towards free-standing high-performance anodes for lithium-ion batteries, Carbon 82 (2015) 337–345.

[108] J.C. Guo, X.L. Chen, C.S. Wang, Carbon scaffold structured silicon anodes for lithium-ion batteries, J. Mater. Chem. 20 (2010) 5035–5040.

[109] H.R. Zhang, X.Y. Qin, J.X. Wu, Y.B. He, H.D. Du, B.H. Li, F.Y. Kang, Electrospun core-shell silicon/carbon fibers with an internal honeycomb-like conductive carbon framework as an anode for lithium ion batteries, J. Mater. Chem. A 3 (2015) 7112–7120.

[110] H.C. Tao, L.Y. Xiong, S.C. Zhu, X.L. Yang, L.L. Zhang, Flexible binder-free reduced graphene oxide wrapped Si/carbon fibers paper anode for high-performance lithium ion batteries, Int. J. Hydrogen Energy 41 (2016) 21268–21277.

[111] R. Nava, L. Cremar, V. Agubra, J. Sanchez, M. Alcoutlabi, K. Lozano, Centrifugal spinning: an alternative for large scale production of silicon-carbon composite nanofibers for lithium ion battery anodes, Acs Appl. Mater. Inter. 8 (2016) 29365–29372.

[112] V.A. Agubra, L. Zuniga, D. Flores, H. Campos, J. Villarreal, M. Alcoutlabi, A comparative study on the performance of binary SnO2/NiO/C and Sn/C composite nanofibers as alternative anode materials for lithium ion batteries, Electrochim. Acta 224 (2017) 608–621.
[113] H.L. Lv, S. Qiu, G.X. Lu, Y. Fu, X.Y. Li, C.X. Hu, J.R. Liu, Nanostructured antimony/carbon composite fibers as anode material for lithium-ion battery, Electrochim. Acta 151 (2015) 214–221.
[114] H. Liu, G.X. Wang, J.Z. Wang, D. Wexler, Magnetite/carbon core-shell nanorods as anode materials for lithium-ion batteries, Electrochem. Commun. 10 (2008) 1879–1882.
[115] G. Bieker, M. Winter, P. Bieker, Electrochemical in situ investigations of SEI and dendrite formation on the lithium metal anode, PCCP 17 (2015) 8670–8679.
[116] M. Akia, L. Cremar, M. Chipara, E. Munoz, H. Cortez, H. de Santiago, F. J. Rodriguez-Macias, Y.I. Vega-Cantu, H. Arandiyan, H.Y. Sun, T.P. Lodge, Y. B. Mao, K. Lozano, In situ production of graphene-fiber hybrid structures, Acs Appl. Mater. Int. 9 (2017) 25474–25480.
[117] A. Manthiram, Electrical energy storage: materials challenges and prospects, MRS Bull. 41 (2016) 624–630.
[118] M. Zhang, T. Wang, G. Cao, Promises and challenges of tin-based compounds as anode materials for lithium-ion batteries, Int. Mater. Rev. 60 (2015) 330–352.
[119] M. Inukai, A. Valdez, L. Zuniga, M. Alcoutlabi, Forcespinning: An alternative method to produce Metal-oxides/Carbon composite fibers as anode materials for Lithium-ion batteries, ECS Trans. 77 (2017) 383–390.
[120] A. Valdez, J. Villarreal, L. Zuniga, M. Alcoutlabi, MoS2 and MoO2 loaded Carbon Microfibers as Anode Materials for Lithium-Ion and Sodium-Ion Batteries, ECS Trans. 85 (2018) 357–368.
[121] H.L. Lyu, J.R. Liu, S. Qiu, Y.H. Cao, C.X. Hu, S.M. Guo, Z.H. Guo, Carbon composite spun fibers with in situ formed multicomponent nanoparticles for a lithium-ion battery anode with enhanced performance, J. Mater. Chem. A 4 (2016) 9881–9889.
[122] M. Akia, N. Salinas, S. Luna, E. Medina, A. Valdez, J. Lopez, J. Ayala, M. Alcoutlabi, K. Lozano, In situ synthesis of Fe3O4-reinforced carbon fiber composites as anodes in lithium-ion batteries, J. Mater. Sci. 54 (2019) 13479–13490.
[123] L. Zuniga, G. Gonzalez, R.O. Chavez, J.C. Myers, T.P. Lodge, M. Alcoutlabi, Centrifugally spun alpha-Fe2O3/TiO2/carbon composite fibers as anode materials for lithium-ion batteries, Appl. Sci.-Basel. 9 (2019).
[124] J.C. Park, J. Kim, H. Kwon, H. Song, Gram-scale synthesis of Cu2O nanocubes and subsequent oxidation to cuo hollow nanostructures for lithium-ion battery anode materials, Adv. Mater. 21 (2009) 803.
[125] E. Zhou, C.G. Wang, M.H. Shao, X.L. Deng, X.J. Xu, MoO2 nanoparticles grown on carbon fibers as anode materials for lithiumion-batteries, Ceram. Int. 43 (2017) 760–765.
[126] X. Zhang, P.S. Kumar, V. Aravindan, H.H. Liu, J. Sundaramurthy, S.G. Mhaisalkar, H.M. Duong, S. Ramakrishna, S. Madhavi, Electrospun TiO2-graphene composite nanofibers as a highly durable insertion anode for lithium ion batteries, J. Phys. Chem. C 116 (2012) 14780–14788.
[127] Y.Y. Zhang, Y.X. Tang, W.L. Li, X.D. Chen, Nanostructured TiO2-based anode materials for high-performance rechargeable lithium-ion batteries, ChemNanoMat 2 (2016) 764–775.
[128] B. Wang, J.L. Cheng, Y.P. Wu, D. Wang, D.N. He, Porous NiO fibers prepared by electrospinning as high performance anode materials for lithium ion batteries, Electrochem. Commun. 23 (2012) 5–8.
[129] X.Z. Shi, S. Zhang, X.C. Chen, T. Tang, R. Klingeler, E. Mijowska, Ultrathin NiO confined within hollow carbon sphere for efficient electrochemical energy storage, J. Alloy. Compd. 797 (2019) 702–709.
[130] S.Y. Wei, D. Di Lecce, R. Brescia, G. Pugliese, P.R. Shearing, J. Hassoun, Electrochemical behavior of nanostructured NiO@C anode in a lithium-ion battery using LiNi1/3Co1/3Mn1/3O2 cathode, J. Alloy. Compd. 844 (2020).
[131] L.W. Ji, Z. Lin, M. Alcoutlabi, O. Toprakci, Y.F. Yao, G.J. Xu, S.L. Li, X.W. Zhang, Electrospun carbon nanofibers decorated with various amounts of electrochemically-inert nickel nanoparticles for use as high-performance energy storage materials, RSC Adv. 2 (2012) 192–198.
[132] Y. Yu, L. Gu, C.B. Zhu, P.A. van Aken, J. Maier, Tin nanoparticles encapsulated in porous multichannel carbon microtubes: preparation by single-nozzle electrospinning and application as anode material for high-performance li-based batteries, J. Am. Chem. Soc. 131 (2009) 15984-+.
[133] D. Bresser, F. Mueller, M. Fiedler, S. Krueger, R. Kloepsch, D. Baither, M. Winter, E. Paillard, S. Passerini, Transition-metal-doped zinc oxide nanoparticles as a new lithium-ion anode material, Chem. Mater. 25 (2013) 4977–4985.
[134] L. Qiao, X.H. Wang, L. Qiao, X.L. Sun, X.W. Li, Y.X. Zheng, D.Y. He, Single electrospun porous NiO-ZnO hybrid nanofibers as anode materials for advanced lithium-ion batteries, Nanoscale 5 (2013) 3037–3042.
[135] X.Y. Shen, D.B. Mu, S. Chen, R. Huang, F. Wu, Electrospun composite of ZnO/Cu nanocrystals-implanted carbon fibers as an anode material with high rate capability for lithium ion batteries, J. Mater. Chem. A 2 (2014) 4309–4315.
[136] J. Lopez, J. Villarreal, J. Cantu, J. Parsons, M. Alcoutlabi, Metal sulfide/carbon composite fibers as anode materials for lithium ion batteries, ECS Trans. 85 (2018) 275–284.
[137] R. Zhou, J.G. Wang, H.Z. Liu, H.Y. Liu, D.D. Jin, X.R. Liu, C. Shen, K.Y. Xie, B. Q. Wei, Coaxial MoS2@Carbon hybrid fibers: a low-cost anode material for high-performance li-ion batteries, Materials 10 (2017).
[138] K. Chang, W.X. Chen, L-cysteine-assisted synthesis of layered MoS2/graphene composites with excellent electrochemical performances for lithium ion batteries, ACS Nano 5 (2011) 4720–4728.
[139] L. Zhang, D. Sun, J. Kang, J. Feng, H.A. Bechtel, L.W. Wang, E.J. Cairns, J.H. Guo, Electrochemical reaction mechanism of the MoS2 electrode in a lithium-ion cell revealed by in situ and operando x-ray absorption spectroscopy, Nano Lett. 18 (2018) 1466–1475.
[140] Y.M. Chen, X.Y. Yu, Z. Li, U. Paik, X.W. Lou, Hierarchical MoS2 tubular structures internally wired by carbon nanotubes as a highly stable anode material for lithium-ion batteries, Sci. Adv. 2 (2016).
[141] A. Manthiram, Y.Z. Fu, Y.S. Su, Challenges and prospects of lithium-sulfur batteries, Accounts Chem. Res. 46 (2013) 1125–1134.
[142] A. Chaturvedi, E. Edison, N. Arun, P. Hu, C. Kloc, V. Aravindan, S. Madhavi, Two dimensional TiS2 as a promising insertion anode for na-ion battery, Chemistryselect 3 (2018) 524–528.
[143] W. Sun, L.M. Suo, F. Wang, N. Eidson, C.Y. Yang, F.D. Han, Z.H. Ma, T. Gao, M. Zhu, C.S. Wang, "Water-in-Salt" electrolyte enabled LiMn2O4/TiS2 Lithium-ion batteries, Electrochem. Commun. 82 (2017) 71–74.
[144] C.L. Tan, Z.Y. Zeng, X. Huang, X.H. Rui, X.J. Wu, B. Li, Z.M. Luo, J.Z. Chen, B. Chen, Q.Y. Yan, H. Zhang, Liquid-phase epitaxial growth of two-dimensional semiconductor hetero-nanostructures, Angew. Chem. Int. Ed. 54 (2015) 1841–1845.
[145] Y.R. Liang, W.H. Lai, Z.C. Miao, S.L. Chou, Nanocomposite materials for the sodium-ion battery: a review, Small 14 (2018).
[146] H.S. Hou, X.Q. Qiu, W.F. Wei, Y. Zhang, X.B. Ji, Carbon anode materials for advanced sodium-ion batteries, Adv. Energy Mater. 7 (2017).
[147] V. Deimede, C. Elmasides, Separators for lithium-ion batteries: a review on the production processes and recent developments, Energy Technol-Ger 3 (2015) 453–468.
[148] Z.F. Dai, U. Mani, H.T. Tan, Q.Y. Yan, Advanced cathode materials for sodium-ion batteries: what determines our choices? Small Methods 1 (2017).
[149] J.F. Huang, Z.W. Xu, L.Y. Cao, Q.L. Zhang, H.B. Ouyang, J.Y. Li, Tailoring MoO2/graphene oxide nanostructures for stable high-density sodium-ion battery anodes, Energy Technol.-Ger 3 (2015) 1108–1114.
[150] H. Jia, M. Dirican, C. Aksu, N. Sun, C. Chen, J.D. Zhu, P. Zhu, C.Y. Yan, Y. Li, Y. Q. Ge, J.S. Guo, X.W. Zhang, Carbon-enhanced centrifugally-spun SnSb/carbon microfiber composite as advanced anode material for sodium-ion battery, J. Colloid Interface Sci. 536 (2019) 655–663.
[151] H. Jia, M. Dirican, J.D. Zhu, C. Chen, C.Y. Yan, P. Zhu, Y. Li, J.S. Guo, Y. Caydamli, X.W. Zhang, High-performance SnSb@rGO@CMF composites as anode material for sodium-ion batteries through high-speed centrifugal spinning, J. Alloy. Compd. 752 (2018) 296–302.
[152] H. Jia, M. Dirican, C. Chen, J.D. Zhu, P. Zhu, C.Y. Yan, Y. Li, X. Dong, J.S. Guo, X. W. Zhang, Reduced graphene oxide-incorporated SnSb@CNF composites as anodes for high-performance sodium-ion batteries, Acs Appl. Mater. Interface 10 (2018) 9696–9703.
[153] Y. Lu, M. Yanilmaz, C. Chen, M. Dirican, Y.Q. Ge, J.D. Zhu, X.W. Zhang, Centrifugally Spun SnO2 microfibers composed of interconnected nanoparticles as the anode in sodium-ion batteries, Chemelectrochem 2 (2015) 1947–1956.
[154] Y. Lu, K. Fu, J.D. Zhu, C. Chen, M. Yanilmaz, M. Dirican, Y.Q. Ge, H. Jiang, X. W. Zhang, Comparing the structures and sodium storage properties of centrifugally spun SnO2 microfiber anodes with/without chemical vapor deposition, J. Mater. Sci. 51 (2016) 4549–4558.
[155] D.T. Ma, Y.L. Li, H.W. Mi, S. Luo, P.X. Zhang, Z.Q. Lin, J.Q. Li, H. Zhang, Robust SnO2-x nanoparticle-impregnated carbon nanofibers with outstanding electrochemical performance for advanced sodium-ion batteries, Angew. Chem. Int. Ed. 57 (2018) 8901–8905.
[156] C.T. Zhao, C. Yu, M.D. Zhang, H.W. Huang, S.F. Li, X.T. Han, Z.B. Liu, J. Yang, W. Xiao, J.N. Liang, X.L. Sun, J.S. Qiu, Ultrafine MoO2-carbon microstructures enable ultralong-life power-type sodium ion storage by enhanced pseudocapacitance, Adv. Energy Mater. 7 (2017).
[157] Z. Liu, T. Song, J.H. Kim, Z.P. Li, J. Xiang, T. Lu, U. Paik, Partially reduced SnO2 nanoparticles anchored on carbon nanofibers for high performance sodium-ion batteries, Electrochem. Commun. 72 (2016) 91–95.
[158] L. Li, Z. Chen, H. Zhang, Z.J. Zhu, M. Zhang, The double effects of sulfur-doping on MoO2/C nanofibers with high properties for Na-ion batteries, Appl. Surf. Sci. 455 (2018) 343–348.
[159] H.K. Wang, Q.Z. Wu, D.X. Cao, X. Lu, J.K. Wang, M.K.H. Leung, S.D. Cheng, L. Lu, C.M. Niu, Synthesis of SnSb-embedded carbon-silica fibers via electrospinning: effect of TEOS on structural evolutions and electrochemical properties, Mater. Today Energy 1–2 (2016) 24–32.
[160] Q.H. Tian, Z.X. Zhang, L. Yang, S. Hirano, Synthesis of SnO2/Sn@carbon nanospheres dispersed in the interspaces of a three-dimensional SnO2/Sma. carbon nanowires network, and their application as an anode material for lithium-ion batteries, J. Mater. Chem. A 2 (2014) 12881–12887.
[161] Y.-H.-Z. Ying Kang, Q.i. Shi, H. Shi, Dongfeng Xue, fa-nian sh, highly efficient Co3O4/CeO2 heterostructure as anode for lithium-ion batteries, J Colloid Interf. Sci. (2020).
[162] P.C. Lian, X.F. Zhu, S.Z. Liang, Z. Li, W.S. Yang, H.H. Wang, High reversible capacity of SnO2/graphene nanocomposite as an anode material for lithium-ion batteries, Electrochim. Acta 56 (2011) 4532–4539.
[163] H. Peng, Y. Liu, S. Ramakrishna, Recent development of centrifugal electrospinning, J. Appl. Polym. Sci. 134 (2017).